New Phytologist

How evolution repeatedly builds complexity: a case study with C_4 photosynthesis in *Blepharis* (Acanthaceae)

Matt Stata[1], Ming-Ju Amy Lyu[2], Hongbing Liu[3], Shifeng Cheng[3], Xin-Guang Zhu[2], Tammy L. Sage[1] and Rowan F. Sage[1]

[1]Department of Ecology and Evolutionary Biology, the University of Toronto, 25 Willcocks Street, Toronto, ON, M5S 3B2, Canada; [2]Center of Excellence for Molecular Plant Sciences, Institute for Plant Physiology and Ecology, Chinese Academy of Sciences, Shanghai, 200032, China; [3]Shenzhen Branch, Guangdong Laboratory for Lingnan Modern Agriculture, Genome Analysis Laboratory of the Ministry of Agriculture, Agricultural Genomics Institute at Shenzhen, Chinese Academy of Agricultural Sciences, Shenzhen, 518120, China

Authors for correspondence:
Matt Stata
Email: matt.stata@alumni.utoronto.ca; *statamat@msu.edu*; *mattstata@gmail.com*

Rowan F. Sage
Email: r.sage@utoronto.ca

Received: *4 March 2025*
Accepted: *26 June 2025*

New Phytologist (2025) **248:** 2092–2110
doi: 10.1111/nph.70426

Key words: *Blepharis* phylogeny, C_3–C_4 intermediates, C_4 photosynthesis, convergent evolution, gas exchange, photosynthetic evolution.

Summary

- With over 60 parallel origins representing evolutionary replicates, C_4 photosynthesis is well-suited for studying complex trait evolution. However, lineages with diverse C_3–C_4 intermediate species are scarce, leaving uncertainty in models of C_4 evolution.
- Phenotypic characterization of 28 living species of *Blepharis* (Acanthaceae) is presented, including photosynthetic gas exchange, enzyme activity assays, cell ultrastructure, and $\delta^{13}C$ assays, the latter including 92 herbarium specimens from three species with phenotypic diversity. A well-resolved transcriptome-based phylogeny provides evolutionary context.
- C_3, proto-Kranz, C_2, C_4-like, and C_4 phenotypes occur in *Blepharis* sect. *Acanthodium*. The phylogeny supports a stepwise progression from C_3 through C_2 to C_4 states and up to five distinct origins of the C_4 cycle. Substantial intraspecific C_2–C_4 variation is demonstrated in *Blepharis mitrata*, *Blepharis furcata*, and *Blepharis macra*. *Blepharis gazensis* is a monospecific C_4 lineage exhibiting an NADP malic enzyme C_4 pathway with features of the NAD-ME subtype, extending the ways in which the C_4 cycle is known to function.
- Substantial photosynthetic diversity exists in *Blepharis* that rivals or exceeds the range of character states present in other C_3 to C_4 transitional lineages. This diversity in *Blepharis* represents a robust new model for studying convergent evolution of C_4 photosynthesis and complex traits in general.

Introduction

Darwin's 'endless forms most beautiful' in the living world are the result of eons of evolutionary innovation characterized by the emergence of increasing complexity (Darwin, 1859). Complex traits create novel ecological opportunities and promote diversification (Yoder *et al.*, 2010; Stroud & Losos, 2016). Although it may seem that complex traits are difficult to evolve and should arise infrequently, numerous examples of their convergent evolution exist (Conway Morris, 2003; Losos, 2018). One of the best is C_4 photosynthesis, a CO_2-concentrating mechanism (CCM) in terrestrial plants that emerged over 60 times despite requiring modification of hundreds or even thousands of genes (Sage, 2016; Niklaus & Kelly, 2019). Convergent evolution enables comparative methods, with independent lineages treated as natural replicates (Harmon, 2018) and facilitates investigation of the core requirements of a complex phenotype as well as the extent to which the underlying mechanisms also converge (Losos, 2011; Khoshravesh *et al.*, 2020a). Species exhibiting both phenotypic and phylogenetic intermediacy are particularly useful, as these may represent ancestral states which have persisted to the present (Monson *et al.*, 1984; Sage *et al.*, 2012; Lundgren *et al.*, 2015). Phenotypically intermediate species occur in about one-quarter of all C_4 lineages, making C_4 photosynthesis a rich case to study how evolution builds complexity. In most C_4 lineages in which intermediates occur, however, there are typically only a few intermediate species, most of which have the same phenotype. An important exception is *Flaveria* (Asteraceae), which is considered a model genus for C_4 evolution due to the presence of numerous intermediate states (Ku *et al.*, 1983, 1991; McKown *et al.*, 2005; Schulze *et al.*, 2013; Adachi *et al.*, 2023). The grass *Alloteropsis semialata* has also risen to prominence due to the discovery of C_3, C_4, and intermediate genotypes or subspecies (Lundgren *et al.*, 2016, 2019; Dunning *et al.*, 2019; Pereira *et al.*, 2023). However, unanswered questions in C_4 evolution require additional intermediate-rich clades to enable robust comparative analyses (Stata *et al.*, 2019). The genus *Blepharis* (Acanthaceae) is particularly promising, with Fisher *et al.* (2015) hypothesizing the presence of dozens of intermediate species, more than found in any other C_4 lineage.

Present address: Matt Stata, Biochemistry and Molecular Biology, Michigan State University, 603 Wilson Road, East Lansing, MI 48824, USA.

Most C_3–C_4 intermediate species exhibit a phenotype now known as C_2 photosynthesis, although these have historically been referred to simply as C_3–C_4 intermediates (Edwards & Ku, 1987; Sage *et al.*, 2014). The core modification in C_2 photosynthesis is the restriction of the photorespiratory enzyme glycine decarboxylase (GDC) to vascular sheath cells, typically the bundle sheath (BS), which forces photorespiratory glycine produced in the mesophyll (M) tissue to diffuse into the BS for decarboxylation, facilitating concentration and refixation of CO_2 in the BS (Sage *et al.*, 2012). C_2 species exhibit photosynthetic CO_2 compensation points (Γ) and O_2 inhibition of net CO_2 assimilation rates that are intermediate between C_3 and C_4 values (Ku *et al.*, 1983, 1991; Khoshravesh *et al.*, 2016, 2020b; Adachi *et al.*, 2023). Although metabolically simpler than C_4 photosynthesis, the C_2 CCM enhances photosynthesis at low intercellular CO_2 concentration (C_i) and is hypothesized to establish a biochemical and structural foundation for assembling the C_4 pathway (Rawsthorne, 1992; Sage *et al.*, 2014). Because the C_2 phenotype is considered to be relatively stable and adaptive in its own right, research addressing C_4 evolution has shifted to consider how C_2 photosynthesis evolved from C_3 and, in turn, how the C_4 cycle emerges from the C_2 state (Heckmann *et al.*, 2013; Sage *et al.*, 2014). Addressing these transitions requires the discovery of more C_3–C_2 and C_2–C_4 intermediates.

While close C_2 relatives have been documented in numerous C_4 lineages, until recently there has been a scarcity of intermediate phenotypes reflecting the C_3 to C_2 and C_2 to C_4 transitions. In the past 20 years, the number of species known to exhibit intermediate character states has increased, particularly those spanning the C_3 and C_2 phenotypes, informing models of how the C_2 pathway evolved. A distinctive C_3 to C_2 intermediate phenotype proposed to be an early stage of C_2 evolution is the proto-Kranz phenotype, which was first recognized in *Euploca* (Boraginaceae; Muhaidat *et al.*, 2011) and has since been identified in the eudicot lineages *Flaveria* (Asteraceae; Sage *et al.*, 2013; Adachi *et al.*, 2023), *Salsola* (Amaranthaceae; Voznesenskaya *et al.*, 2013), and *Tribulus* (Zygophyllaceae; Leung *et al.*, 2024), as well as the grass lineages *Steinchisma*, *Neurachne*, and *Homolepis* (Poaceae; Khoshravesh *et al.*, 2016, 2020b; Alvarenga *et al.*, 2025). The proto-Kranz condition is characterized by increased abundance of organelles in the BS and centripetal localization of BS mitochondria. These patterns are hypothesized to enhance refixation of photorespired CO_2 in the BS and to facilitate the subsequent establishment of the C_2 pathway by creating selection for reduction of GDC in M cells (Sage *et al.*, 2012). Concordantly, the discovery of incomplete, sub-C_2 phenotypes in *Flaveria* (Sage *et al.*, 2013; Adachi *et al.*, 2023), *Neurachne* (Khoshravesh *et al.*, 2020b), *Tribulus* (Leung *et al.*, 2024), and *Homolepis* (Alvarenga *et al.*, 2025), supports a hypothesis that restriction of GDC to the BS occurs gradually.

In contrast to C_2 photosynthesis, which primarily requires the loss of GDC from M cells, the transition from C_2 to C_4 photosynthesis necessitates cell-specific upregulation of multiple enzymes and transporters along with the integration of the C_4 and photosynthetic carbon reduction (PCR) cycles (Monson *et al.*, 1986; Moore *et al.*, 1988). Two identified phenotypes representing stages during the C_2–C_4 transition were historically known as Type II C_2 (or simply Type II C_3-C_4) and C_4-like photosynthesis. Whereas typical (Type I) C_2 species lack significant C_4 cycle activity, Type II C_2 species exhibit moderate upregulation of some C_4 cycle enzymes (Edwards & Ku, 1987; Adachi *et al.*, 2023). However, the nascent, incomplete C_4 cycle in these species contributes little to net CO_2 assimilation (Monson *et al.*, 1986, 1988; Edwards & Ku, 1987; Alonso-Cantabrana & von Caemmerer, 2016; Adachi *et al.*, 2023). In contrast, C_4-like species have a strong and well-integrated C_4 cycle yet retain some Rubisco activity and C_3 photosynthesis in M cells (Monson *et al.*, 1987; Cheng *et al.*, 1988; Moore *et al.*, 1989; Monson & Rawsthorne, 2000). The clearest examples of C_2–C_4 intermediate phenotypes occur only in *Flaveria* (*F. ramosissima*, Type II C_2, and *F. brownii*, C_4-like; Adachi *et al.*, 2023). The scarcity of C_2–C_4 intermediates in other transitional lineages has led to the suggestion that the assembly and integration of the C_4 cycle may have occurred in a punctuated manner, leaving much uncertainty about the key evolutionary steps (Stata *et al.*, 2019). This deficiency is significant, since it represents the entire upregulation and integration of C_4 metabolism. There is thus a need to identify multiple, parallel lineages with a high diversity of intermediate phenotypes, particularly those representing late stages in C_4 evolution. *Blepharis* stands out as uniquely promising due to its large number of putative intermediates, including two possible C_4-like species (Fisher *et al.*, 2015).

Blepharis is an old-world genus of 128 species inhabiting arid regions in Africa, Arabia, and southeast Asia and is classified into three infrageneric groups (Vollesen, 2000). C_4 photosynthesis, first reported in *B. scindica* in 1975, has also been characterized in *B. attenuata* and *B. ciliaris* (Sankhla *et al.*, 1975; Muhaidat *et al.*, 2007; Akhani *et al.*, 2008). Based on $\delta^{13}C$ data, Fisher *et al.* (2015) identified 13 C_4 *Blepharis* species, all within section *Acanthodium*. Based on anatomical observations of herbarium specimens, they hypothesized many of the remaining 44 sect. *Acanthodium* species could be intermediates, including the two putative C_4-like species; however, the lack of live plants prevented confirmation of intermediate physiology. This study examines the physiological and anatomical diversity of 28 *Blepharis* species. We integrate gas exchange measurements, $\delta^{13}C$ analysis, enzyme assays, ultrastructural observations, and transcriptome-based phylogenetic inference. We also include a comprehensive phylogenetic network analysis to investigate evidence of hybridization in *Blepharis* (Supporting Information Notes S1). In addition, we present analysis of $\delta^{13}C$ values from 98 herbarium accessions of three *Blepharis* species in which our physiological assays detected C_4 and non-C_4 phenotypes. Our results show that *Blepharis* is a remarkably dynamic C_3–C_4 transitional lineage, with diverse photosynthetic phenotypes including C_2–C_4 intermediacy, multiple origins of C_4 photosynthesis, and a previously unknown variant of the C_4 pathway.

Nomenclature of C_3–C_4 intermediates

The historical terminology surrounding C_3–C_4 intermediacy suffers from a lack of evolutionary clarity, with the C_4-like and Type

I and II C_2 terms being particularly ambiguous. To resolve these nomenclatural issues, a simple, logical scheme of trait progression from the C_3 to C_4 character states has been proposed (Leung *et al.*, 2024; Alvarenga *et al.*, 2025), where:

$$C_3 \rightarrow C_{3^+} \rightarrow \text{proto}-\text{Kranz} \rightarrow C_{2^-} \rightarrow C_2 \rightarrow C_{2^+} \rightarrow C_{4^-} \rightarrow C_4$$

In this nomenclature, a '+' represents an augmentation to a typical C_3 or C_2 character state that can facilitate transition to the next character state, while a '−' represents an incomplete expression of the next character state in the transition. Character states that appear to mark major stages in the transition are given distinctive descriptors, such as proto-Kranz or C_2. The former Type I C_2 intermediate would be simply C_2, while the Type II intermediate augmented with a nascent C_4 cycle is a C_2+. C_4-like species such as *F. brownii* are now classified as C_4− (= sub-C_4 in Alvarenga *et al.*, 2025), reflecting that they are largely C_4 in function but lack key features such as complete compartmentalization of Rubisco and the C_3 pathway into the BS tissue. Similarly, C_2 species with incomplete GDC localization to the BS are classified as C_2− (= sub-C_2 in Alvarenga *et al.*, 2025). As new character states are discovered, they can readily be slotted into this scheme, and if sufficiently distinctive, they could be given their own designation. In this study of *Blepharis*, we follow this nomenclature.

Materials and Methods

Plant materials and growth conditions

Seeds were collected from field sites or herbarium samples as outlined in Table S1, which also includes all species authority information; Fig. S1 provides images of species in their native habitats. In general, germination was rapid (about a day), and seeds did not require special treatments as they are explosively released from their capsules upon hydration (Gutterman, 1993). Even in the case of seeds from herbarium specimens or seed libraries, if the seeds were viable, germination was rapid and easy, with no age-induced dormancy or recalcitrance. We also found that seeds could be desiccated and frozen without loss of viability for longer term storage. Plants were grown in a glasshouse at the University of Toronto in 12 L pots with 27–30°C days, 22–25°C nights, and photosynthetic photon flux density (PPFD) of ≥ 1500 µmol m^{-2} s^{-1} on clear days or ≥ 300 µmol m^{-2} s^{-1} on cloudy days supplemented by high-pressure sodium lighting. Plants were grown in a soil blend comprising equal parts sand, vermiculite, topsoil, and ProMix (Premier Tech Home and Garden, QC, Canada) formulated to approximate soil of arid regions with reduced organic content while remaining relatively loose and well-aerated to minimize root rot. Plants were watered daily and fertilized weekly with a 50 : 50 mix of 21-7-7 acid fertilizer and 20-20-20 general-purpose fertilizer, plus a supplement of 30 µM iron Ethylenediamine di(o-hydroxyphenylacetic acid), 1 mM calcium nitrate, and 1 mM magnesium sulfate (Plant Products, ON, Canada). We found the plants easy to maintain under these conditions, provided they did not experience excessive watering or severe drought. Samples for enzyme assays, $\delta^{13}C$, and RNA-seq were collected in the glasshouse. For gas exchange and microscopy, plants were transferred to Conviron PGC20 growth chambers (Conviron Canada, Winnipeg, MB) with 30°C day, 25°C night temperatures, a 13-h photoperiod, and 1100–1200 µmol m^{-2} PPFD at the top of the leaf canopy for 2 wk before analysis. Growth chambers were used to prepare plants for gas exchange analyses because we could maintain constant growth conditions over the lengthy time required to complete the gas exchange measurements (e.g. by maintaining a constant photoperiod). Because sampling for enzyme assays, RNA-seq, and starch $\delta^{13}C$ could each be conducted in a single day but required more space for the complete collection, these were conducted on glasshouse-grown plants in early-to-mid September, when conditions were similar to the growth chambers. All analyses used the most recent fully expanded leaves.

Gas exchange measurements

The response of net CO_2 assimilation rate (A) to intercellular CO_2 concentration (C_i) was measured with an LI-6400XT gas exchange system (LI-COR Biosciences, Lincoln, NE, USA) at a PPFD of 1600 µmol photons m^{-2} s^{-1} and 30°C as described in Table S2. 1600 µmol photons m^{-2} s^{-1} PPFD was selected based on preliminary analyses, which indicated that this intensity was saturating for photosynthesis in all species. Leaf area was measured using ImageJ (Schindelin *et al.*, 2015). Linear regressions were determined using the Python library SciPy's stats.linregress function (Virtanen *et al.*, 2020) through the lowest five C_i values. The CO_2 compensation point of A (Γ) was estimated as the x-intercept of the linear regression, while carboxylation efficiency (CE) was estimated as the slope of the linear regression. The CE values were then normalized to A at saturating CO_2 (A_{1500}). The ratio A_{1500}/A_{400} was used to determine the relative CO_2 saturation at 400 µmol mol^{-1}.

$\delta^{13}C$ analysis

$\delta^{13}C$ of leaf starch was measured from living samples collected on a weekend in early September with a gentle breeze (wind speed of 10–20 km h^{-1} on the Beaufort wind scale) sufficient to mix surface air with bulk atmosphere. Samples were collected between 3 and 6 pm in a well-ventilated glasshouse. These conditions served to maximize leaf starch content, reduce variation in the source gas isotopic ratios, and minimize fossil fuel CO_2 contributions from local traffic. Glasshouse vents were kept partly open for 48 h before sampling so that the difference between indoor and outdoor CO_2 was consistently < 15 µmol mol^{-1}, as measured by two LI-6400XT machines. Leaf starch was used instead of bulk leaf for $\delta^{13}C$ analysis both because accumulated starch primarily represents a single photoperiod while bulk leaf material reflects the entire development time, and because discrimination against ^{13}C by postphotosynthetic processes can skew $\delta^{13}C$ values of bulk leaves by 1–2‰, complicating interspecies comparisons (Adachi *et al.*, 2023). Samples were flash-frozen in liquid nitrogen and stored at −80°C. Starch was extracted

enzymatically (Richter *et al.*, 2009; Adachi *et al.*, 2023), and 150 µl of extract per sample was evaporated in tin capsules (model D1006; Elemental Microanalysis, Okehampton, UK). $\delta^{13}C$ was also measured on 2 mg samples of dried leaf from 92 herbarium specimens of *B. furcata*, *B. macra*, and *B. mitrata* (Table S3). The names for most of these specimens were confirmed by Kai Vollesen, the taxonomic authority for *Blepharis* (Vollesen, 2000). All $\delta^{13}C$ measurements were conducted by the Washington State University Stable Isotope Laboratory (www.isotopes.wsu.edu). Monthly precipitation means were obtained for all herbarium specimen collection locations from WorldClim v.2 (worldclim.org) and summed to annual totals from 1970 to 2000 using the R package geodata. Daily maximum and minimum temperatures from 2010 to 2020 were obtained from NASA POWER (power.larc.nasa.gov) using the R package nasapower and used to calculate growing degree days (GDD) as the sum of $\max(((T_{max} + T_{min})/2) - 10°C, 0)$ over all days.

Enzyme assays

Activity of Rubisco, PEP carboxylase (PEPC), NADP-dependent malate dehydrogenase (MDH), NAD malic enzyme (NAD-ME), NADP malic enzyme (NADP-ME), aspartate aminotransferase (AST), alanine aminotransferase (ALT), and pyruvate phosphate dikinase (PPDK) were assayed at 30°C by coupling the rate of oxidation or reduction of NAD(H) or NADP(H) measured at 340 nm (with a Hewlett–Packard mode 8452A diode array spectrophotometer) to the enzyme activity of interest. Assay protocols followed Ashton *et al.* (1990) and Keys & Parry (1990), with modifications based on testing and other literature (Matsuba *et al.*, 1997; Voznesenskaya *et al.*, 2001; Ueno & Sentoku, 2006; Oakley *et al.*, 2014; Dever *et al.*, 2015; Friesen & Sage, 2016; Adachi *et al.*, 2023) (Table S4). NAD-ME activity was assayed in C_4 and C_4- species only to confirm that NADP-ME is the primary decarboxylase. PEP carboxykinase (PCK) was not assayed because use of this decarboxylase is rare in C_4 eudicots, particularly those in which NADP-ME is the primary decarboxylase. Transcriptome data also support the hypothesis that NADP-ME is the primary decarboxylase in *Blepharis*, as no C_4 *Blepharis* species exhibited upregulation of NAD-ME or PCK (Stata, 2023). Leaf samples were collected from glasshouse-grown plants under bright conditions such that the PPFD was near 1500 µmol m^{-2} s^{-1}, flash-frozen in liquid N_2, and stored at −80°C until assayed. Samples were homogenized using an electric drill-powered tissue grinder (model 358111; DWK Life Science, Millville, NJ, USA) with 1 ml of extraction buffer per square centimeter of leaf. All assays were conducted on the same extract in the following sequence: PPDK, PEPC, NADP-ME, NAD-ME (if performed), Rubisco, AST, ALT, and NADP-MDH. Chl was quantified spectrophotometrically (Arnon, 1949). Only PPDK was found to lose activity over the time from extraction to final assay; hence, it was always run first. NADP-MDH was always run last as it requires incubation at a high concentration of DTT to obtain maximum activity. All other enzymes showed stable activity. Due to lack of detectable NAD-ME activity in *Blepharis* species, the NAD-ME assay was validated using leaf samples from the known NAD-ME C_4 species *Gynandropsis gynandra* (Cleomaceae) and *Amaranthus retroflexus* (Amaranthaceae), which were grown in a glasshouse at the University of Toronto.

Phylotranscriptomic inference

Phylogenetic inferences were based on transcriptome assemblies of live plants and short-read genomic DNA data for transcriptome specimens and *B. dhofarensis* (Table S5). Leaf samples were flash-frozen and stored at −80°C. RNA was extracted using PureLink kits (Thermo Fisher Scientific, Waltham, MA, USA) and assessed using an Agilent 2100 Bioanalyzer (Agilent Technologies, Santa Clara, CA, USA). cDNA libraries were constructed using the NEBNext Ultra II kit (New England Biolabs, Ipswich, MA, USA) and sequenced using the Illumina Novaseq 6000 platform (Illumina, San Diego, CA, USA) with paired-end 150-bp reads by Berry Genomics (berrygenomics.com). RNA-seq data for five additional Acanthaceae outgroup species were downloaded from the NCBI SRA (Table S5). Reads were trimmed based on quality using Trimmomatic (Bolger *et al.*, 2014) with minimum leading and trailing quality cutoffs of 30, a five-base sliding window cutoff of 30, and a minimum length of 70 bp.

Transcriptome assembly, ortholog detection, and single-copy ortholog processing were conducted as described by Adachi *et al.* (2023). Software tools and version information are provided in Table S6 (Rice *et al.*, 2000; Suyama *et al.*, 2006; Capella-Gutiérrez *et al.*, 2009; Grabherr *et al.*, 2011; Katoh & Standley, 2013; Zhang *et al.*, 2018; Emms & Kelly, 2019; Kim *et al.*, 2019; Kozlov *et al.*, 2019; Danecek *et al.*, 2021). The criteria for selecting low-copy orthogroups were a maximum of eight missing taxa and a maximum of 10% of taxa with multiple sequences permitted before an entire orthogroup was rejected. A gap tolerance for alignment trimming of 0.8 was used. Following this procedure, 5377 low-copy orthogroups were identified, of which 3670 remained after fragment assembly and paralog removal; from these, 2461 with alignment lengths between 500 and 2500 bp were selected for further analysis.

Short-read genomic DNA data were generated for herbarium specimens, and *B. dhofarensis* (Table S5) was prepared using the DNA Nanoball (DNB) protocol as previously described (Liu *et al.*, 2024) and read-map pileups for reference-based assembly were generated as described in Adachi *et al.* (2023; software details in Table S6). A Python script was used to generate reference-based assemblies as follows: at each site in a pileup, either the most abundant base in the mapped reads was selected, or an N was called if three or fewer reads mapped to that site, or if the frequency of the second most abundant base was $> 75\%$ of that of the top base, indicating either heterozygosity or multiple paralogs. If $> 1\%$ of sites were considered heterozygous in this manner, the entire sequence was rejected due to the likelihood of paralogs.

After final filtering to remove orthogroups with more than eight missing taxa, 2138 orthogroups were selected for phylogenetic analysis, representing 2.78 megabases. Phylogenetic analysis based on concatenated supermatrix and multispecies coalescent approaches was conducted as described by Adachi *et al.* (2023; software details in Table S6). All taxa and assembly methodologies are listed in Table S5.

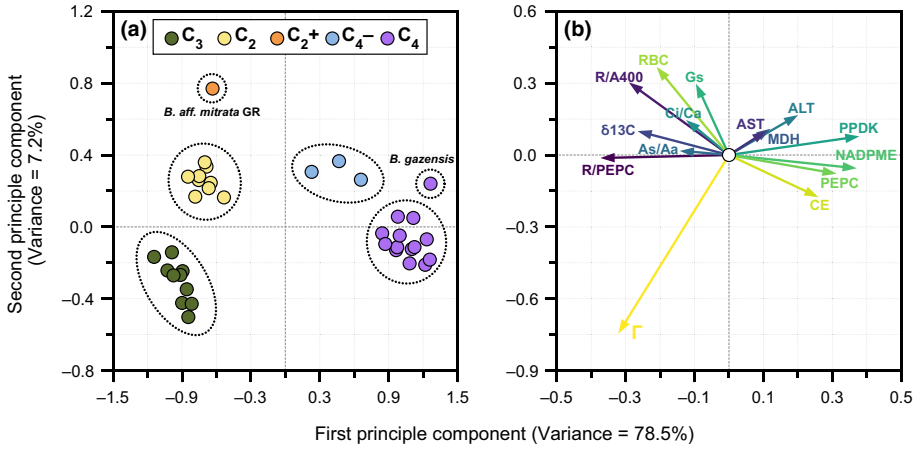

Fig. 1 Principal component analysis and k-means clustering of physiological data in 37 *Blepharis* species and populations. C_3, C_2, C_2+, C_4−, and C_4 species separate into clusters when plotted on the first two principal components (a). A machine learning k-means clustering algorithm ($n = 6$) identifies the same clusters (dotted ellipses), with the unusual C_2 population of *Blepharis mitrata* from Graaff-Reinet (denoted C_2+) and the C_4 species *Blepharis gazensis* each forming a single-member cluster. (b) The individual data variables plotted as vectors in PC space: ALT, alanine aminotransferase activity; A_s/A_a, the ratio of net CO_2 assimilation at saturating (1500 μmol mol^{-1}) over A at ambient (400 μmol mol^{-1}) CO_2; AST, aspartate aminotransferase activity; CE, carboxylation efficiency normalized to A_s; C_i/C_a, the ratio of intercellular CO_2 to ambient CO_2; $\delta^{13}C$, carbon isotope ratio; g_s, stomatal conductance; MDH, NADP-dependent malate dehydrogenase activity; NADP-ME, NADP malic enzyme activity; PEPC, phosphoenolpyruvate carboxylase activity; PPDK, pyruvate, phosphate dikinase activity; R/A_{400}, the ratio of Rubisco activity to net CO_2 assimilation at 400 μmol mol^{-1}; R/PEPC, the ratio of the activity of Rubisco to PEPC; RBC, Rubisco activity; Γ, CO_2 compensation point.

Leaf microscopy

Qualitative features of leaf anatomy and ultrastructural features of BS cells were assessed from leaf tissue sampled halfway up the leaf and halfway between the midrib and leaf margin of the most recently expanded leaf. Tissue samples were taken between 30 min and 2 h from the start of the photoperiod, fixed initially with 1% glutaraldehyde (v/v), 4% (w/v) paraformaldehyde, post-fixed in osmium tetroxide, and embedded in Araldite as described previously (Khoshravesh *et al.*, 2017). Light micrographs were taken using a Ziess Axiophot equipped with a DP71 Olympus camera and Olympus CellSens image software (Advanced Microscopy Techniques, Woburn MA, USA). A Philips 201 transmission electron microscope (TEM) equipped with an Advantage HR camera system (Advanced Microscopy Techniques) was used to capture TEM micrographs. To ensure selection of representative images, qualitative observations of leaf anatomy and ultrastructure were made on leaves from three different plants. Observations of BS ultrastructure were made on five BS cells from one leaf each from three different plants.

Statistical analysis

A principal component analysis (PCA) and k-means clustering were conducted using all collected physiological data as features (Tables S7–S9) using the Python module Scikit-learn (MacQueen, 1967; Pedregosa *et al.*, 2011). Because datasets frequently lacked normal distributions, analysis of variation was conducted using the Kruskal–Wallis nonparametric test (Kruskal & Wallis, 1952) followed by Conover *post hoc* tests for statistical groupings (Conover & Iman, 1979). Linear regression analyses and A/C_i curve fitting were conducted in Python using SciPy (Virtanen *et al.*, 2020). To visually simplify numerous A/C_i curves, data were fitted to the function $y = (P_1x)/(x + P_2) + P_3$ using the SciPy.optimize.curve_fit function with P_1, P_2, and P_3 as tunable parameters. Significance of linear regressions was assessed using the Wald test as implemented in the SciPy.stats.linregress function. Regressions are presented with residual bootstrapping showing uncertainty or variability in the regression and prediction intervals within which 95% of new observations are expected to occur. Sample sizes for all analyses are presented in the associated figure and table legends.

Results

PCA and phenotypic classification

To objectively categorize the unstudied photosynthetic diversity in *Blepharis*, we first conducted a PCA using our physiological data (Tables S7–S9). Principal components 1 and 2 explained 79% and 7% of total variation, respectively, and discrete clusters were identified corresponding to C_3, C_2, C_4−, and C_4 taxa (Fig. 1a). The machine learning algorithm k-means (MacQueen, 1967) supported six distinct phenotypic categories including C_3, C_2, C_4−, and C_4.

There are also two single-sample clusters: a *Blepharis mitrata* accession from Graaff-Reinet, South Africa, which is C_2 but with a low, C_4-like Γ and elevated C_4 enzyme activity, which we categorize as C_2+; and *Blepharis gazensis*, a C_4 species with atypically high ALT, AST, and NADP-MDH activities (Fig. 1a, dotted ellipses; Tables S7–S9). Reducing the number of k-means clusters had the following effects: with five clusters, *B. mitrata* Graaff-

Table 1 Carbon isotope ratio and gas exchange properties in 28 species of *Blepharis*, grouped by photosynthetic category.

Physiology	Carbon isotope ratio $\delta^{13}C$ (‰)	CO_2 compensation point Γ (μmol mol^{-1})	Carboxylation efficiency	A_{1500}/A_{400}	C_i/C_a	A400 (μmol m^{-2} s^{-1})	g_s (mol m^{-2} s^{-1})
C_3 (10)	−27.7 ± 1.0 a	55.3 ± 2.9 a	4.7 ± 0.6 a	1.81 ± 0.33 a,b	0.73 ± 0.06 a	22.1 ± 5.7 a	0.50 ± 0.23 a
C_2 (9)	−28.5 ± 0.8 b	14.9 ± 4.7 b	4.3 ± 0.6 a	1.79 ± 0.19 a	0.76 ± 0.05 a,b	26.1 ± 2.1 a	0.63 ± 0.11 a
C_4− (3)	−17.5 ± 0.4 c	0.8 ± 0.2 c	9.6 ± 1.2 b	1.48 ± 0.04 b	0.66 ± 0.07 b	23.0 ± 4.6 a	0.34 ± 0.04 b
C_4 (14)	−12.9 ± 1.2 d	0.3 ± 0.7 d	17.8 ± 5.3 c	1.10 ± 0.05 c	0.53 ± 0.04 c	31.1 ± 4.2 b	0.33 ± 0.06 b

Mean ± SD. Carboxylation efficiency is normalized to the net CO_2 assimilation rate at 1500 μmol CO_2 mol^{-1} air. Letters denote statistical groupings for each measurement based on Kruskal–Wallis one-way analysis of variance followed by Conover's *post hoc* test using Holm–Bonferroni P-adjustment. The outlier C_2+ population of *B. mitrata* from Graaff-Reinet is omitted from the C_2 category. Numbers in parentheses next to photosynthetic categories denote the number of species/populations in each category; see Supporting Information Table S7 for individual values.

Table 2 Activity of Rubisco and C_4 cycle enzymes in 28 species of *Blepharis*, grouped by photosynthetic category.

Physiology	Rubisco	PEPC	NADP-ME	PPDK	NADP-MDH	AST	ALT
Rates by Chl (mmol mol_{chl}^{-1} s^{-1})							
C_3 (10)	106.6 ± 17.3 a	24.8 ± 9.4 a	1.5 ± 0.8 a	0.7 ± 0.5 a	23.9 ± 11.0 a	40.3 ± 12.9 a	97.8 ± 23.2 a
C_2 (9)	129.0 ± 31.0 a	43.6 ± 7.9 b	3.6 ± 1.9 b	0.9 ± 0.7 a	34.0 ± 13.8 a	67.6 ± 26.8 b	140.9 ± 32.2 b
C_4− (3)	100.0 ± 2.6 a	456.1 ± 119.1 c	141.2 ± 48.4 c	44.5 ± 10.9 b	92.9 ± 8.6 b	148.3 ± 14.7 c	568.4 ± 125.2 c
C_4 (13)	45.8 ± 7.6 b	709.5 ± 180.4 d	164.3 ± 28.3 c	39.7 ± 10.2 b	121.0 ± 27.1 b	166.6 ± 24.8 c	416.1 ± 77.4 c
Rates by leaf area (μmol m^{-2} s^{-1})							
C_3 (10)	53.7 ± 19.9 a	12.2 ± 4.1 a	0.6 ± 0.2 a	0.4 ± 0.3 a	12.0 ± 4.9 a	19.1 ± 4.4 a	47.7 ± 13.3 a
C_2 (9)	58.8 ± 9.6 a	20.2 ± 4.2 b	1.6 ± 0.8 b	0.4 ± 0.4 a	16.0 ± 7.3 a	29.9 ± 8.0 b	66.8 ± 22.2 a
C_4− (3)	47.6 ± 4.6 a	210.3 ± 41.3 c	65.7 ± 21.0 c	20.8 ± 5.2 b	43.6 ± 4.7 b	69.3 ± 4.4 c	261.3 ± 38.6 b
C_4 (13)	25.0 ± 6.2 b	379.6 ± 107.6 d	90.0 ± 23.8 c	20.8 ± 4.2 b	65.1 ± 14.6 b	91.1 ± 18.1 d	228.2 ± 57.9 b

Mean ± SD. Letters denote statistical groupings for each enzyme based on Kruskal–Wallis one-way analysis of variance followed by Conover's *post hoc* test using Holm–Bonferroni P-adjustment and a corrected *P*-value cutoff for significance of 0.05. The outlier C_2+ population of *B. mitrata* from Graaff-Reinet is omitted from the C_2 category. *Blepharis gazensis* is omitted from the C_4 category for NADP-MDH, AST, and ALT due to outlier values. Numbers in parentheses next to photosynthetic categories denote the number of species/populations in each category; see Supporting Information Tables S8 and S9 for individual values.

Reinet joined the C_2 cluster; with four, *B. gazensis* joined the C_4 cluster; and with three, the C_4 and C_4− clusters merged (not shown). PCA variables plotted as vectors (Fig. 1b) show that PC1 is primarily influenced by C_4 cycle enzyme activities, $\delta^{13}C$, and Γ, while PC2 is most influenced by Γ, stomatal conductance (g_s), and Rubisco activity. The phenotypic classifications established here were used for all subsequent statistical analyses (Tables 1–2, S2, S7–S9).

Photosynthetic gas exchange and leaf starch $\delta^{13}C$ analyses

Mean A/C_i curves for representative C_3, C_2, C_4−, and C_4 *Blepharis* species illustrate the range of photosynthetic responses to C_i (Fig. 2a). For improved visibility, fitted curves, both raw and normalized, were generated for the full A/C_i dataset (Fig. 2b, c). C_2 species show responses similar to those of C_3 species but with lower Γ. C_4 species have Γ values near zero and sharp initial responses saturating at 200–300 μmol CO_2 mol^{-1} air (Fig. 2b). All three *B. furcata* (C_4−) accessions have normalized responses intermediate between the C_4 and non-C_4 curves (Fig. 2c). Normalized CE values for *B. furcata* are statistically intermediate between C_4 and non-C_4 species, while higher A_{1500}/A_{400} indicates CO_2 saturation occurs at higher C_i than in C_4 species (Tables 1, S7; Fig. S2).

Blepharis leaf starch $\delta^{13}C$ values from living specimens showed distinct variation between photosynthetic groups (Tables 2, S7). C_3 and C_4 groups had typical values of −27.7 and 12.9‰, respectively. The C_2 mean was 0.8‰ more negative than C_3 species, while the C_4− mean of −17.5‰ was intermediate between C_3 and C_4 values. Gas exchange metrics were plotted against leaf starch $\delta^{13}C$ to evaluate their relationship with the strength of C_4 metabolism as indicated by less negative $\delta^{13}C$ values (Fig. 3; Table S7). Less negative $\delta^{13}C$ values indicate C_4 cycle engagement because PEPC has lower discrimination against ^{13}C than Rubisco (Monson *et al.*, 1988; von Caemmerer, 1992). This is evident in the linear relationship ($R^2 = 0.84$) between $\delta^{13}C$ and PEPC activity, especially in the intermediate C_4− types (Fig. 3f). C_2 species show a marked reduction in Γ and a small but significant shift to more negative $\delta^{13}C$ values compared with C_3 plants (Fig. 3b; Table 1). The C_2+ Graaff-Reinet population of *B. mitrata* has a low, C_4-like Γ but a C_3-like $\delta^{13}C$ value, in contrast to the typically C_4 values in the two Pofadder accessions of *B. mitrata* (Table S7). All C_4− *B. furcata* accessions have C_4 Γ and intermediate $\delta^{13}C$ values (Fig. 3b; Table S7). *Blepharis furcata* accessions have higher A_{1500}/A_{400} and C_i/C_a values and lower normalized CE, compared with fully C_4 species (Fig. 3b–d; Tables 1, S7); these characters do not significantly differ between C_2 and C_3 species (Table 1). Stomatal conductance (g_s) was

New Phytologist

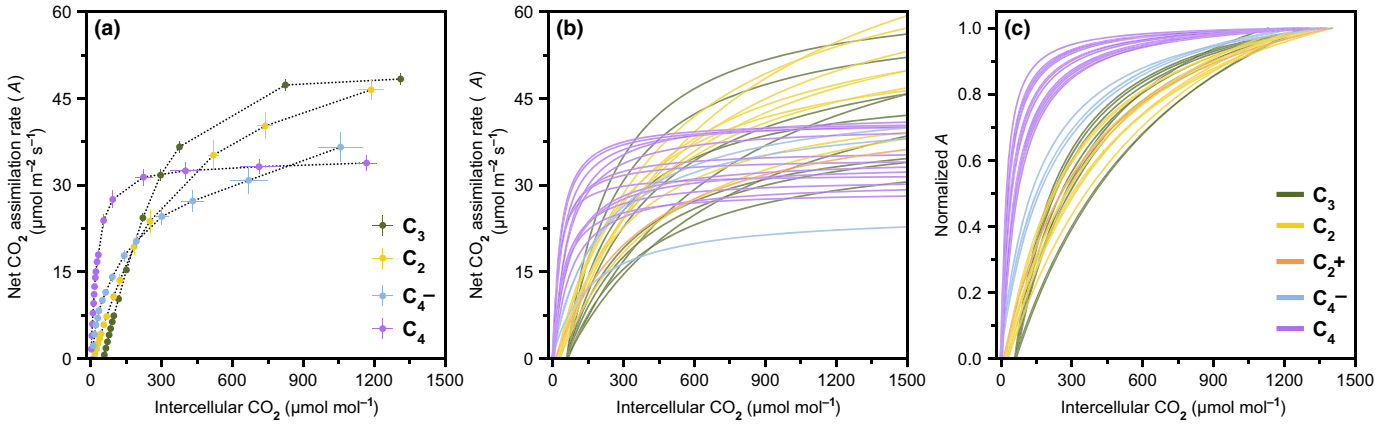

Fig. 2 Net CO_2 assimilation rate (A) to intercellular CO_2 (C_i) response curves in 37 *Blepharis* species and populations. Panel (a) presents A/C_i curves for a representative species from each physiological type (C_3, *B. spinifex* MSB; C_2, *B. diversispina* S24A; C_4-, *B. furcata* Richtersveld; C_4, *B. aspera* S23). $\bar{x}$ = SE, $n = 5$. In (b), A/C_i curves for the 37 species and populations measured (Supporting Information Table S7) are shown with fitted functions [$y = (P_1x)/(x + P_2) + P_3$]. Panel (c) shows fitted and normalized A/C_i curves of all species and populations, obtained by dividing the A values of each curve by its maximum value.

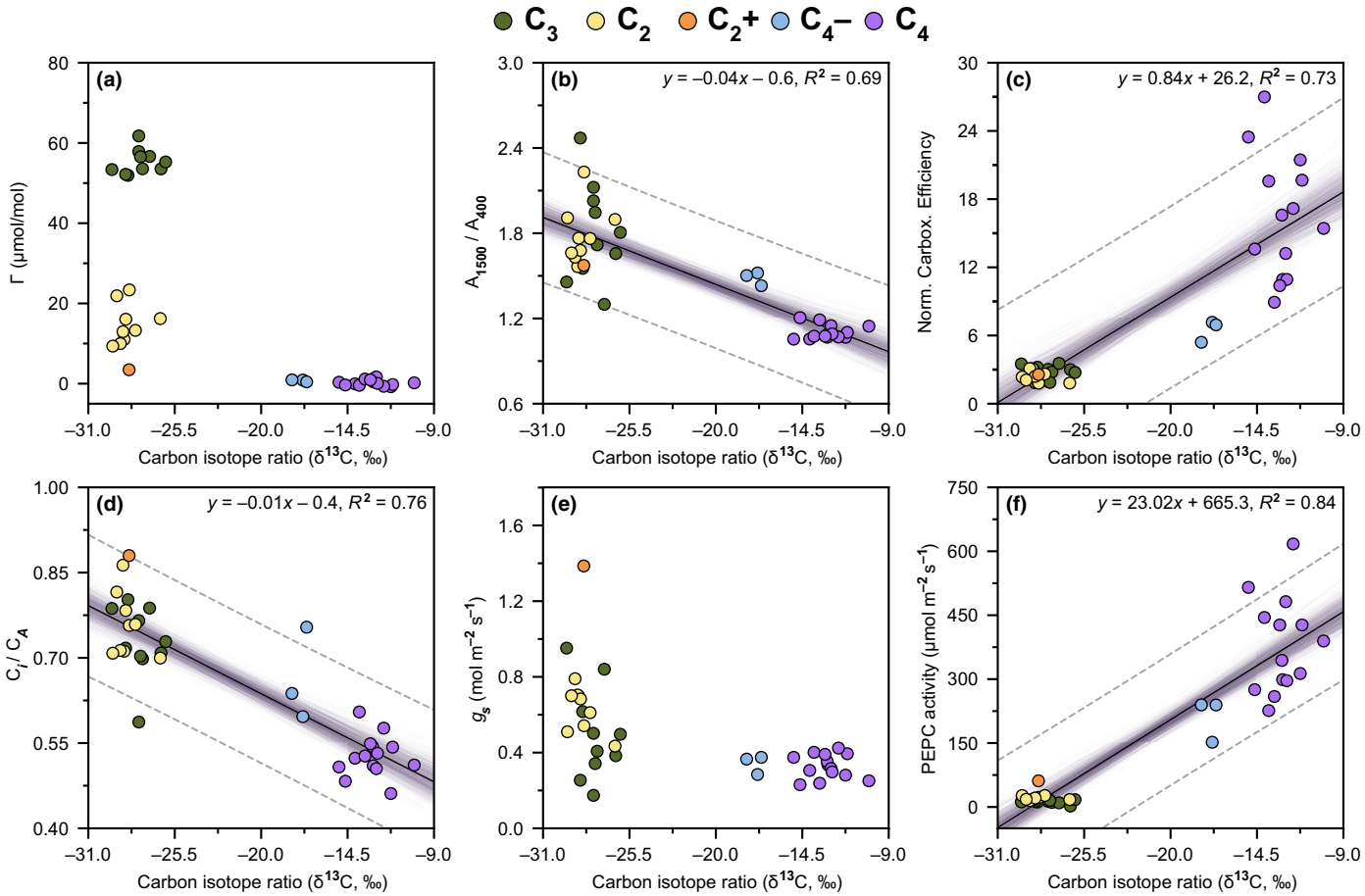

Fig. 3 Relationship between carbon isotope ratio and gas exchange parameters in 37 *Blepharis* species and populations. Relationships are shown between $\delta^{13}C$ and (a) the CO_2 compensation point of the net CO_2 assimilation rate (Γ); (b) the ratio of net CO_2 assimilation rate at 1500–400 ppm CO_2 ($A_s : A_{400}$); (c) the carboxylation efficiency normalized to A_{400}; (d) the ratio of intercellular CO_2 to ambient CO_2 ($C_i : C_a$); (e) stomatal conductance, g_s; (f) PEP carboxylase activity on a leaf area basis. Dashed gray lines denote the prediction interval within which 95% of new observations are expected to occur, and the regression uncertainty is shown using 1000 residual bootstraps (shaded region). Only regressions that were significant (Wald test; $P < 0.05$) are shown.

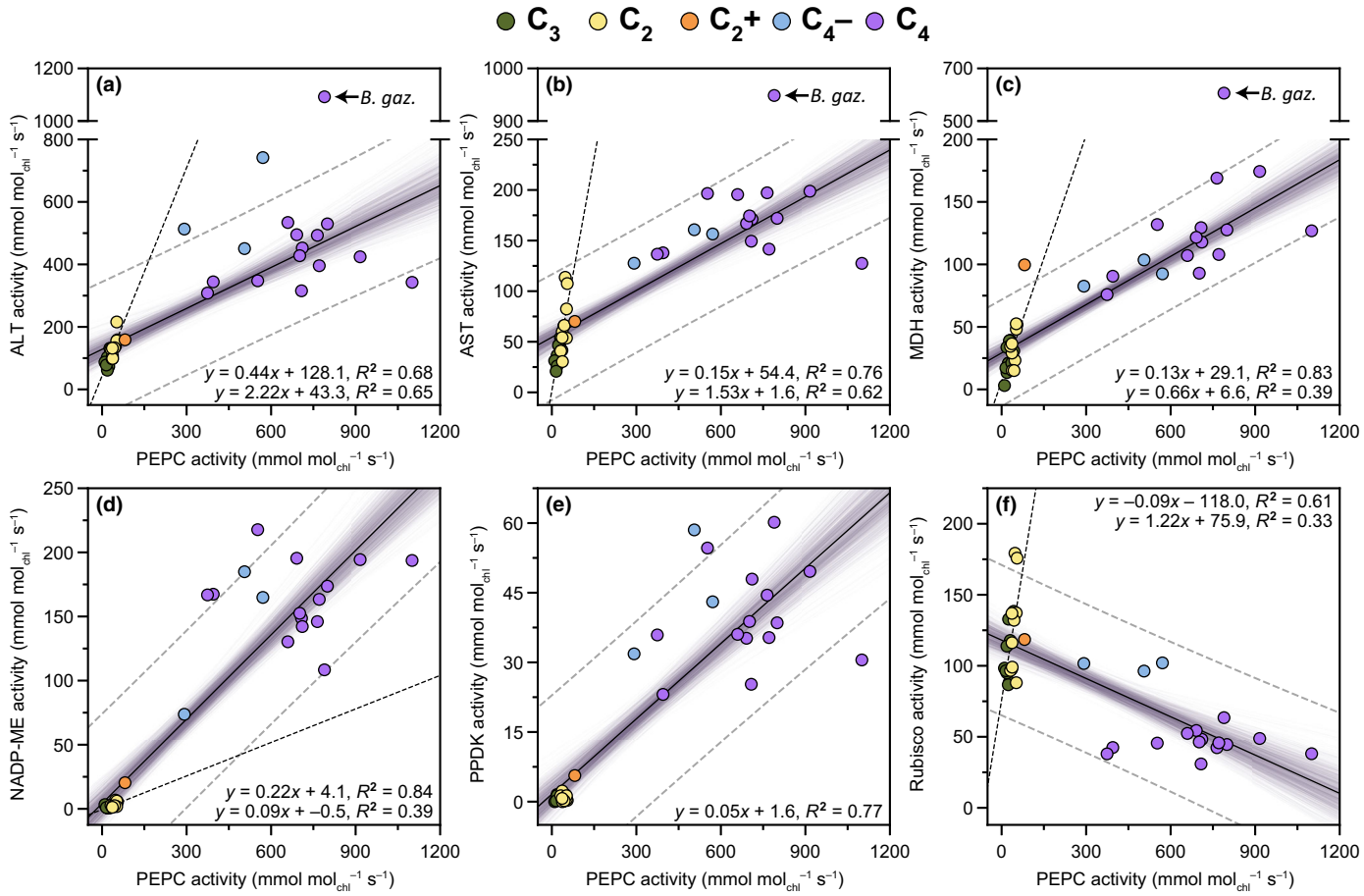

Fig. 4 Relationship between the activity of PEPC and other enzymes in 37 *Blepharis* species and populations. The relationship between the activity of PEP carboxylase (PEPC) and (a) alanine aminotransferase (ALT); (b) aspartate aminotransferase (AST); (c) NADP-dependent malate dehydrogenase (MDH); (d) NADP malic enzyme (NADP-ME); (e) pyruvate, phosphate dikinase (PPDK); and (f) Rubisco. Dashed gray lines denote the prediction interval within which 95% of new observations are expected to occur, and the regression uncertainty is shown using 1000 residual bootstraps (shaded region). Because *B. gazensis* represents a distinct C_4 lineage (Figs 1, 8) and is an outlier in (a–c), it is omitted from the regression analyses here. Significant regressions (Wald test, $P < 0.05$) are shown for the entire dataset (solid black lines) and for C_3 and C_2 taxa only (a–d and f, black dashed lines; excluding *B. mitrata* from Graaff-Reinet). Plots for C_3–C_2 regressions and tables of individual values are presented in Supporting Information Fig. S3.

generally lower in C_4 and C_4- species than in C_3 and C_2 plants (Fig. 3e; Table 1), resulting in higher intrinsic water use efficiency (A_{400}/g_s; Fig. S2). *Blepharis dhofarensis* (C_3) showed low C_i/C_a (0.59) and high A_{400}/g_s (80 μmol mol^{-1}) driven by very low g_s, which probably explains the more positive $\delta^{13}C$ values observed in this arborescent arid-land species than in the other C_3 *Blepharis* species (Table S7).

Leaf biochemistry

All C_4 and C_4- *Blepharis* species showed high activities of NADP-ME (Tables 2, S8–S9; Fig. S2). NAD-ME activity was undetectable in *Blepharis*, whereas rates for the known NAD-ME species *G. gynandra* (Cleomaceae) and *A. retroflexus* (Amaranthaceae) were 84.2 ± 4.3 and 36.9 ± 5.1 mmol mol$_{chl}^{-1}$ s^{-1}, respectively (mean ± SE; $n = 3$), demonstrating the assay worked well. Negligible NAD-ME activity was also observed for *B. ciliaris*, despite this species previously being identified as NAD-ME by western blot analysis (Akhani *et al.*, 2008). We suspect that the NADP-ME antibody used by Akhani *et al.* (2008), which was raised against *Zea mays*, likely had had low binding affinity for the *Blepharis* NADP-ME, resulting in lack of detection. The activities of examined C_4 cycle enzymes were positively correlated with PEPC activity, while Rubisco was negatively correlated (Fig. 4). Among C_3 and C_2 species, all enzyme rates except PPDK correlate positively with PEPC (Figs 4, S3). C_2 species also showed higher average PEPC, NADP-ME, AST, and ALT activities than C_3 species (Table 2; Figs S2–S3). The C_4 species *B. gazensis* exhibited ALT, AST, and NADP-MDH rates far exceeding those in other C_4 *Blepharis* species (Fig. 4a–c; Tables S8, S9). Notably, we observed the regressions through the C_3 to C_2 activity data for ALT vs PEPC, AST vs PEPC, and MDH vs PEPC had steeper slopes than the corresponding regressions through all the data, while the regression slopes for Rubisco vs PEPC had opposite directions in the C_3 to C_2 data relative to the C_3 to C_4 data (Figs 4, S3). We hypothesize these shifts reflect a change in selection imperatives during C_3 to C_2 evolution, vs C_2 to C_4 evolution.

All *B. furcata* (C_4−) accessions showed C_4 enzyme rates comparable to or lower than fully C_4 species and higher Rubisco activity similar to C_3 and C_2 species (Table 2). C_2 species had lower activities of C_4 cycle enzymes than C_4− and C_4 species; however, PEPC, NADP-ME, AST, and ALT were elevated relative to C_3 species (Table 2). A similar increase was not observed for PPDK or NADP-MDH, although PEPC and NADP-MDH rates were correlated in C_3 and C_2 species (Table 2; Figs 4, S3). In the Graaff-Reinet accession of *B. mitrata*, activities of PEPC, NADP-ME, PPDK, and NADP-MDH were elevated relative to C_3 and C_2 species, supporting its designation as a C_2+ species but were well below those of C_4+ and C_4 species including the C_4 *B. mitrata* species from Pofadder, SA (Tables S8, S9). The Graaff-Reinet accession of *B. mitrata* exhibited higher rates of PEPC, NADP-MDH, NADP-ME, and PPDK than any of the C_3 or C_2 species (Fig. S2; Tables S8, S9). Statistical grouping for enzyme rates on a Chl basis and a leaf area basis was similar, except for minor changes in AST and ALT (Tables 2, S8, S9).

Leaf anatomy and bundle sheath cell ultrastructure

Qualitative leaf anatomical patterns in *Blepharis* follow a similar pattern to those reported for other C_3, proto-Kranz, C_2, C_4−, and C_4 eudicots (Figs 5–7, S4; McKown & Dengler, 2007; Muhaidat *et al.*, 2011; Sage *et al.*, 2011; Leung *et al.*, 2024). While *Blepharis* species may differ in having unifacial or bifacial leaves, BS cells form a complete sheath around the vascular tissue in all species examined (Figs 5, S4). The BS cells of *B. leendertziae* (C_3; sect. *Scorpioidea*) and *B. spinifex* (C_3; sect. *Acanthodium*) are typical of C_3 plants, with few mitochondria and chloroplasts, most of which are localized to the BS periphery (Panels a and b in Figs 5–7). In contrast, BS cells in *B. subvolubilis* (functionally C_3) have centripetal aggregates of chloroplasts and mitochondria (Panel c in Figs 5–7). This characteristic is a key indicator of the proto-Kranz phenotype identified as an early stage of C_3-to-C_2 evolution (Sage *et al.*, 2012). The BS cells of the C_2 species *B. diversispina* and *B. macra* have pronounced centripetal aggregates of chloroplasts and mitochondria, with some chloroplasts also positioned along the outer periphery (Panels d and e in Figs 5–7). Fig. 7(d,e) shows a high magnification of the close positioning present between mitochondria and chloroplasts in the centripetal aggregate of organelles in the BS, which is a characteristic of C_2 species. The BS cells of *B. furcata* (C_4−) resemble C_2 species but have fewer chloroplasts and no mitochondria in the outer periphery and a larger centripetal aggregation of organelles (Panel f in Figs 5–7). The Graaff-Reinet (C_2+) and Pofadder (C_4) accessions of *B. mitrata* differ; in that, the C_4 accession has fewer mitochondria, and all organelles are centripetally aggregated (Panels g and h in Figs 5–7). In both the C_4 *B. mitrata* Pofadder accession and the C_4 species *B. linariifolia*, the centripetal aggregations of organelles have closely spaced, often enlarged and/or elongated chloroplasts, in a pattern often observed in NADP-ME C_4 eudicots (Panels h and i in Figs 5–7; Sage *et al.*, 2014).

Most C_4 *Blepharis* exhibit typical NADP-ME C_4 BS ultrastructure, with few mitochondria and many enlarged chloroplasts with fewer and smaller thylakoid grana stacks (Fig. 5h,i). In contrast to other C_4 *Blepharis*, BS cells of *B. gazensis* have abundant mitochondria and prominent thylakoid grana (Fig. 8). These differences, coupled with high AST, ALT, and NADP-MDH activities (Tables S8, S9), demonstrate functional divergence in *B. gazensis*, highlighted by its distinct clustering in the PCA and k-means plot (Fig. 1a).

$\delta^{13}C$ analysis of herbarium samples

Fisher *et al.* (2015) reported $\delta^{13}C$ values indicative of C_4- phenotypes for *B. furcata* and *B. macra*; however, our live *B. macra* plants exhibited a C_2 phenotype with low C_4 cycle activity. Additionally, we found variation in live accessions of *B. mitrata*, with the Pofadder accessions exhibiting full C_4 photosynthesis while the Graaff-Reinet accession has a C_2+ phenotype. Given this possibility of photosynthetic variation within these species, we measured bulk leaf $\delta^{13}C$ from 92 herbarium specimens of *B. furcata*, *B. macra*, and *B. mitrata* collected across their geographic ranges and compared them with previous *Blepharis* C_3 and C_4 values presented in Fisher *et al.* (2015); Fig. 9; Table S3. *B. mitrata* $\delta^{13}C$ ranged from C_4 (−13‰) to C_3 values (−28‰), with a bimodal distribution. $\delta^{13}C$ ranged from borderline C_4 (−15‰) to higher C_3 (−24‰) in *B. furcata* and from borderline C_4 (−16‰) to typical C_3 (−27‰) in *B. macra* (Fig. 9). We found a significant difference between climate parameters associated with *B. mitrata* specimens with C_4-like $\delta^{13}C$ (< −20‰) vs non-C_4 $\delta^{13}C$ (> −20‰); and specimens with C_4 $\delta^{13}C$ values associated with warmer and drier habitats (as indicated by greater growing degree days and lower mean annual precipitation, respectively; Fig. S5).

Phylogenetic analysis

Transcriptome-based phylogenetic inference produced a robust phylogeny with 100% support at most nodes after removing three hybrid samples (Fig. 10; Notes S1). Both the genus *Blepharis* and sect. *Acanthodium* were resolved as monophyletic, except for *B. dhofarensis*. This arborescent species was previously resolved outside of *Blepharis* (McDade *et al.*, 2005) and likely warrants reclassification within *Acanthus* or as its own genus. Only minor conflicts were observed between the coalescent and concatenation trees (Figs 10, S6).

Based on our phylogeny, we denote six distinct clades in *Blepharis* sect. *Acanthodium*. The C_3 species *B. spinifex* and *B. procumbens* comprise Acanthodium I, which branches basally within sect. *Acanthodium*. Next, Acanthodium II comprises C_3 and C_2 taxa plus the unusual C_4 species *B. gazensis*. Within this clade, *B. subvolubilis* exhibits proto-Kranz anatomy (Fig. 5c), with similar BS ultrastructure observed in *B. stainbankiae* and *B. breyeri* (Stata, 2023). Analysis of DNA from herbarium samples also places *Blepharis espinosa* and *B. meyeri* in this clade; these are both inferred to be C_3 or C_2 based on $\delta^{13}C$ (Fisher *et al.*, 2015). The remaining clades, Acanthodium III through VI, lack confirmed C_3 species, spanning a range of phenotypes from C_2 to C_4. Acanthodium III contains the C_2 species *B. gigantea*,

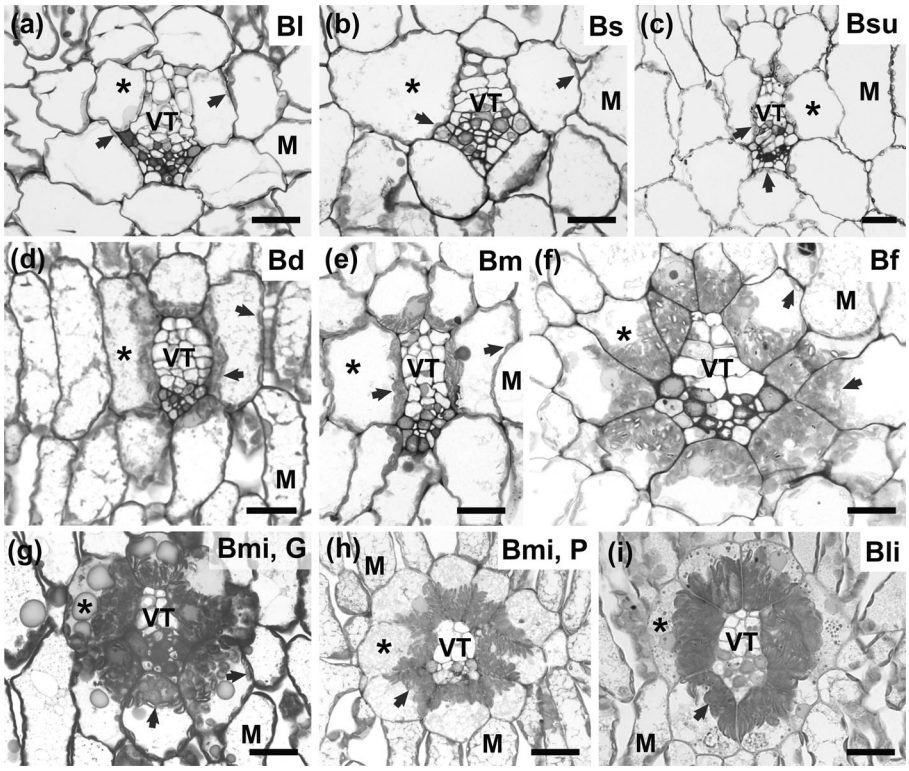

Fig. 5 Light micrographs illustrating cross-sections of a vein from leaves of nine *Blepharis* species with different photosynthetic phenotypes. Panels show (a) *Blepharis leendertziae* (Bl), C_3; (b) *Blepharis spinifex* (Bs), C_3; (c) *Blepharis subvolubilis* (Bsu), C_3 proto-Kranz; (d) *Blepharis diversispina* Tolwe population (Bd), C_2; (e) *Blepharis macra* (Bm), C_2; (f) *Blepharis furcata* Richtersveld population (Bf), C_4-; (g) *Blepharis mitrata* Graaff-Reinet population (Bmi, G), C_2+; (h) *B. mitrata* Pofadder 1 population (Bmi, P), C_4; (i) *B. linariifolia* (Bli), C_4. Bars, 20 μm. M, mesophyll; VT, vascular tissue. Asterisks label mediolateral bundle sheath cells. Arrows mark chloroplasts.

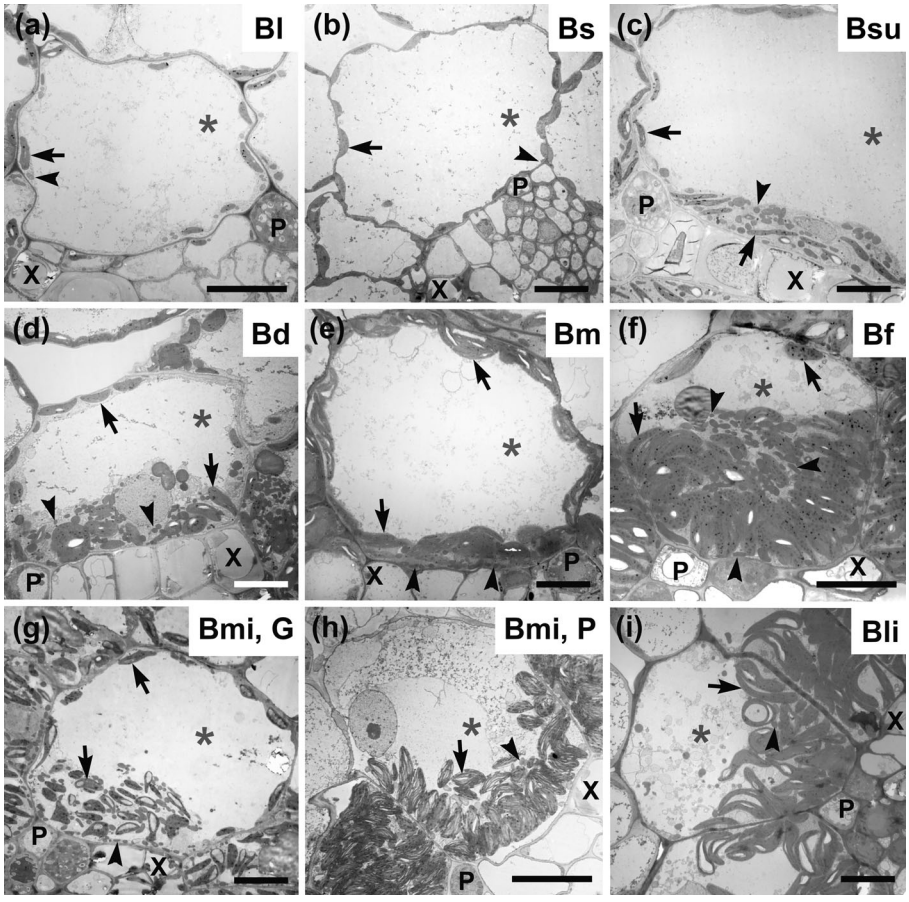

Fig. 6 Transmission electron micrographs illustrating ultrastructure of mediolateral bundle sheath cells for nine *Blepharis* species with different photosynthetic phenotypes. Panels show (a) *Blepharis leendertziae* (Bl), C_3; (b) *Blepharis spinifex* (Bs), C_3; (c) *Blepharis subvolubilis* (Bsu), C_3 proto-Kranz; (d) *Blepharis diversispina* Tolwe population (Bd), C_2; (e) *Blepharis macra* (Bm), C_2; (f) *Blepharis furcata* Richtersveld population (Bf), C_4-; (g) *Blepharis mitrata* Graaff-Reinet population (Bmi, G), C_2+; (h) *B. mitrata* Pofadder 1 population (Bmi, P), C_4; (i) *B. linariifolia* (Bli), C_4. Bars, 10 μm. P, phloem; X, xylem. Asterisks label bundle sheath cells; arrows mark chloroplasts; arrowheads highlight mitochondria.

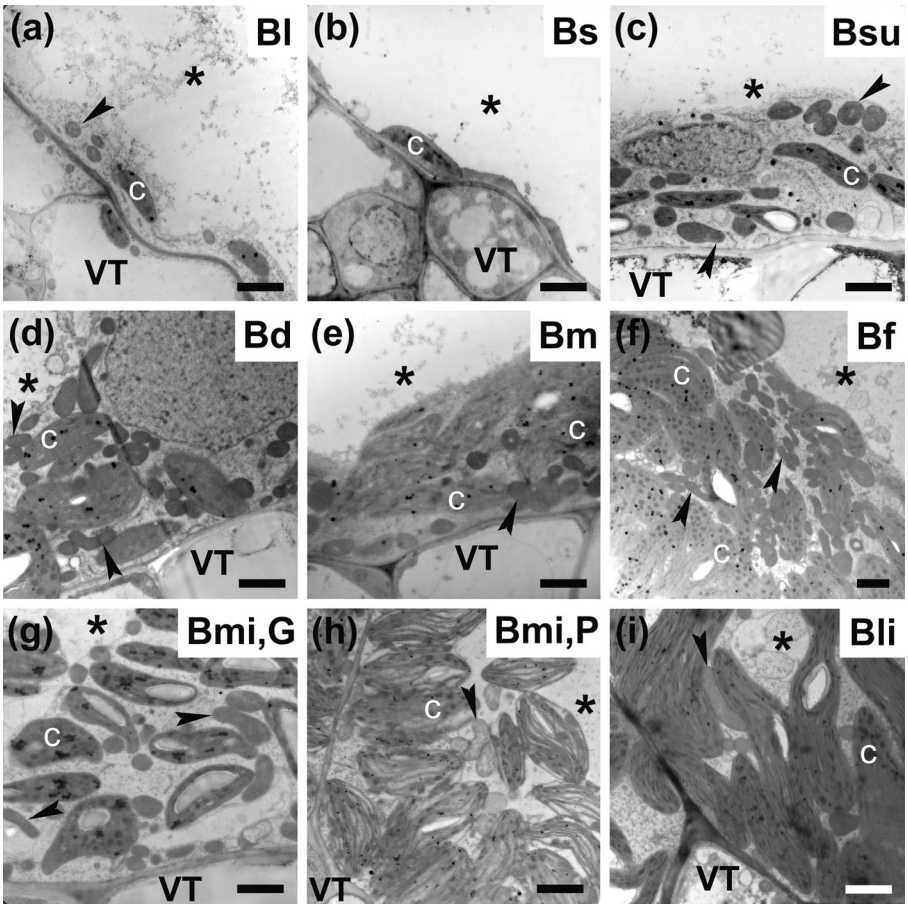

Fig. 7 Transmission electron micrographs highlighting centripetal organelle positioning within mediolateral bundle sheath cells from Fig. 5. Panels show (a) *Blepharis leendertziae* (Bl), C_3; (b) *Blepharis spinifex* (Bs), C_3; (c) *Blepharis subvolubilis* (Bsu), C_3 proto-Kranz; (d) *Blepharis diversispina* Tolwe population (Bd), C_2; (e) *Blepharis macra* (Bm), C_2; (f) *Blepharis furcata* Richtersveld population (Bf), C_4-; (g) *Blepharis mitrata* Graaff-Reinet population (Bmi, G), C_2+; (h) *B. mitrata* Pofadder 1 population (Bmi, P), C_4; (i) *Blepharis linariifolia* (Bli), C_4. Bars, 2 μm. C, chloroplast; VT, vascular tissue. Arrowheads mark mitochondria. Asterisks label bundle sheath cells.

B. pruinosa, and *B. ferox*, and Acanthodium IV represents a C_4 lineage comprised of *B. aspera* and *B. serrulata*. *Blepharis furcata*, *B. macra*, and *B. mitrata* together form Acanthodium V; this clade is particularly noteworthy for its diversity spanning from C_2 to C_4 phenotypes (Fig. 9). Phylogenetic placement and $\delta^{13}C$ (Table S3) indicate that the Werger 325 specimen originally classified as *B. furcata* is likely a misidentified *B. mitrata*. Acanthodium VI comprises all remaining fully C_4 *Blepharis* species and corresponds with the Ciliaris group, which has expanded geographically well beyond the southern African center of diversity for sect. *Acanthodium*, into northern Africa, the Middle East, and northwestern India (Vollesen, 2000; Fisher *et al.*, 2015).

Discussion

Overview of photosynthetic diversity in *Blepharis*

This study reveals rich photosynthetic diversity spanning a range of phenotypes from C_3 to C_4 in *Blepharis* sect. *Acanthodium*. Based on anatomical observations of herbarium materials, Fisher *et al.* (2015) suggested that all members of *Blepharis* sect. *Acanthodium* are C_4, C_4-, or C_2, with a C_2 common ancestor and the closest C_3 sisters being more distantly related infrageneric sections. In our live collection of 42 accessions from 28 species, we demonstrate C_3–C_4 intermediate phenotypes in 12 species or populations of *Blepharis*. We also identified five functionally C_3 species in section *Acanthodium*, including three that exhibit proto-Kranz ultrastructure in the BS. PCA and k-means clustering delineated six distinct functional groups based on the aggregated physiological data. Two of these are monospecific: the *B. mitrata* Graaff-Reinet accession with a strong C_2+ phenotype and the atypical C_4 species *B. gazensis*.

The other clusters represent five C_3 species, eight C_2 species, one C_4- species, and 11 C_4 species. Moreover, our $\delta^{13}C$ survey of nearly 100 herbarium specimens of *B. furcata*, *B. macra*, and *B. mitrata* showed each species includes populations that span the $\delta^{13}C$ range from C_3-like to fully C_4, with numerous accessions in the −22 to −16‰ range corresponding to the C_4- physiology. *Blepharis* sect. *Acanthodium* thus spans a wide range of C_3–C_4 intermediate phenotypes, with notable diversity in the underexplored C_2+ and C_4- conditions representing the later stages of C_4 evolution.

Compared with C_3 species, fully C_4 *Blepharis* have Γ values near zero, elevated CE, and positively shifted $\delta^{13}C$, driven by strong C_4 cycle engagement, while C_2 species are characterized primarily by lower Γ (14.9 ± 4.7 μmol mol^{-1}) than C_3 species (55.3 ± 2.9 μmol mol^{-1}). C_2 species lack the elevated CE and positively shifted $\delta^{13}C$ values observed in C_4 and C_4- species, largely because they lack a strong C_4 cycle that is well-integrated with the PCR cycle in BS tissue (Monson & Rawsthorne, 2000). $\delta^{13}C$ in most C_2 *Blepharis* species is instead shifted negatively compared with C_3 species, reflecting

the double discrimination against $^{13}CO_2$ by BS Rubisco (von Caemmerer, 1989, 1992). The Graaff-Reinet *B. mitrata* accession exhibits a C_2+ phenotype characterized by lower Γ and higher activities of PEPC, NADP-MDH, NADP-ME, and PPDK than other C_2 or C_3 species, despite having C_3-like $\delta^{13}C$ and CE data indicating little C_4PCR cycle integration.

Based on intermediate $\delta^{13}C$ of herbarium specimens, Fisher *et al.* (2015) hypothesized a C_4− phenotype occurs in *B. furcata* and *B. macra*. The accession of *B. macra* studied here exhibited a C_2 phenotype, but broader $\delta^{13}C$ analysis of herbarium specimens indicates intraspecific C_2–C_4 variation exists in this species (will be discussed later). Conversely, high C_4 cycle enzyme activity, elevated CE, lower Γ, and positively shifted $\delta^{13}C$ relative to C_3 and C_2 species demonstrate the presence of a strong, integrated C_4 cycle in all three live accessions of *B. furcata*. However, compared with C_4 *Blepharis*, lower CE and PEPC activity, coupled with higher Rubisco activity and A_{1500}/A_{400}, indicate that C_3 photosynthesis occurs in M cells in *B. furcata*, similar to what has been observed in the C_4− species *Flaveria brownii* (Monson *et al.*, 1987; Cheng *et al.*, 1988; Adachi *et al.*, 2023). A stepwise model of C_4 evolution initially developed for *Flaveria* hypothesizes that restriction of Rubisco to the BS evolves late, after C_4-PCR cycle integration (Sage *et al.*, 2012). The patterns observed in the C_2+ and C_4− accessions of *Blepharis* provide compelling evidence for the broader relevance of the *Flaveria* model of C_4 evolution.

While all other C_4 *Blepharis* species have a typical NADP-ME C_4 phenotype, *B. gazensis* exhibits BS ultrastructure and aminotransferase activities commonly associated with the NADME C_4 pathway. Despite these observations, we detected high NADP-ME activity and no NADME activity in this species. BS cells in *B. gazensis* have abundant mitochondria and prominent thylakoid grana. Because

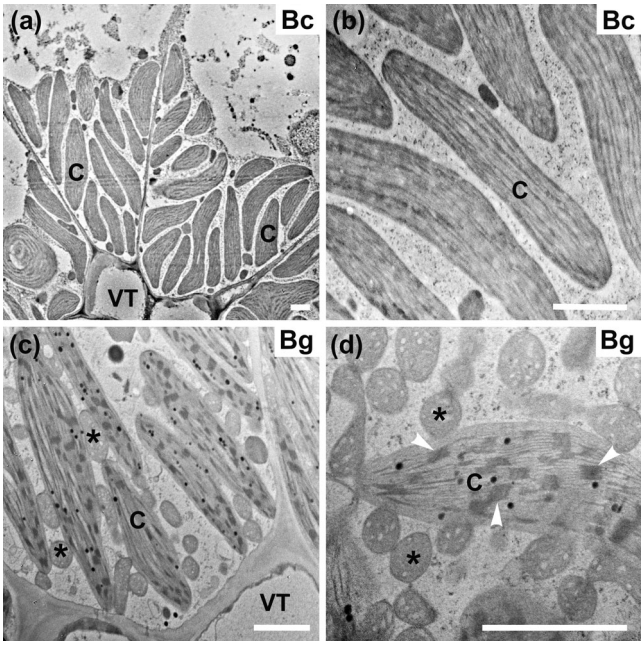

Fig. 8 Transmission electron micrographs of bundle sheath organelles in the C_4 species *Blepharis ciliaris* and *Blepharis gazensis*. Centripetally located bundle sheath chloroplasts and mitochondria are shown for the C_4 species *B. ciliaris* (a, b) and *B. gazensis* (c, d). Bars, 2 μm. C, chloroplast; VT, vascular tissue. Mitochondria are labeled with an asterisk, and white arrowheads denote thylakoid grana stacks.

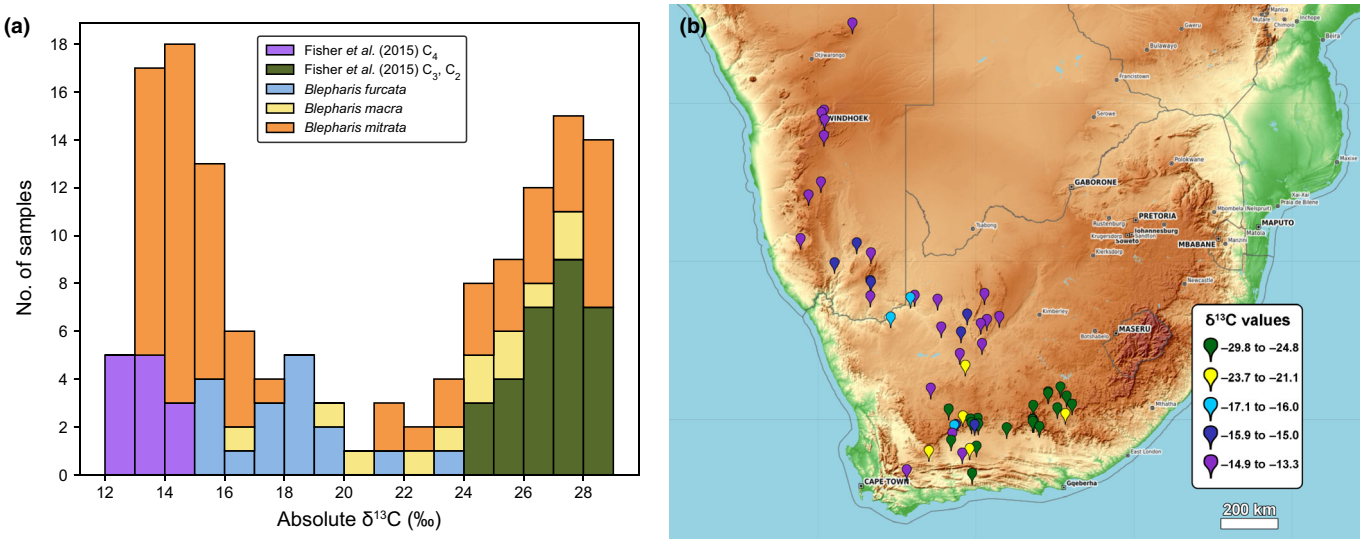

Fig. 9 $\delta^{13}C$ values for 98 herbarium specimens of *Blepharis furcata*, *B. macra*, and *B. mitrata* and geographic locations for 64 *B. mitrata* specimens. (a) A stacked histogram of $\delta^{13}C$ values for populations of *B. furcata* ($n = 18$), *B. macra* ($n = 12$), and *B. mitrata* ($n = 68$), with C_4 and non-C_4 values from Fisher *et al*. (2015) for reference, demonstrates substantial variation in each of these species. (b) A map of collection locations for *B. mitrata* in South Africa and Namibia plotted on a topographical map with $\delta^{13}C$ indicated by point color shows that C_4 populations occur primarily on the Central Plateau (darker tan region), whilenon-C_4 populations are largely restricted to the region along or below the surrounding Great Escarpment. See Supporting Information Fig. S5 for graphs showing precipitation and growing degree days data associated with collection sites for *B. mitrata* specimens with C_4-like vs non-C_4 $\delta^{13}C$ values.

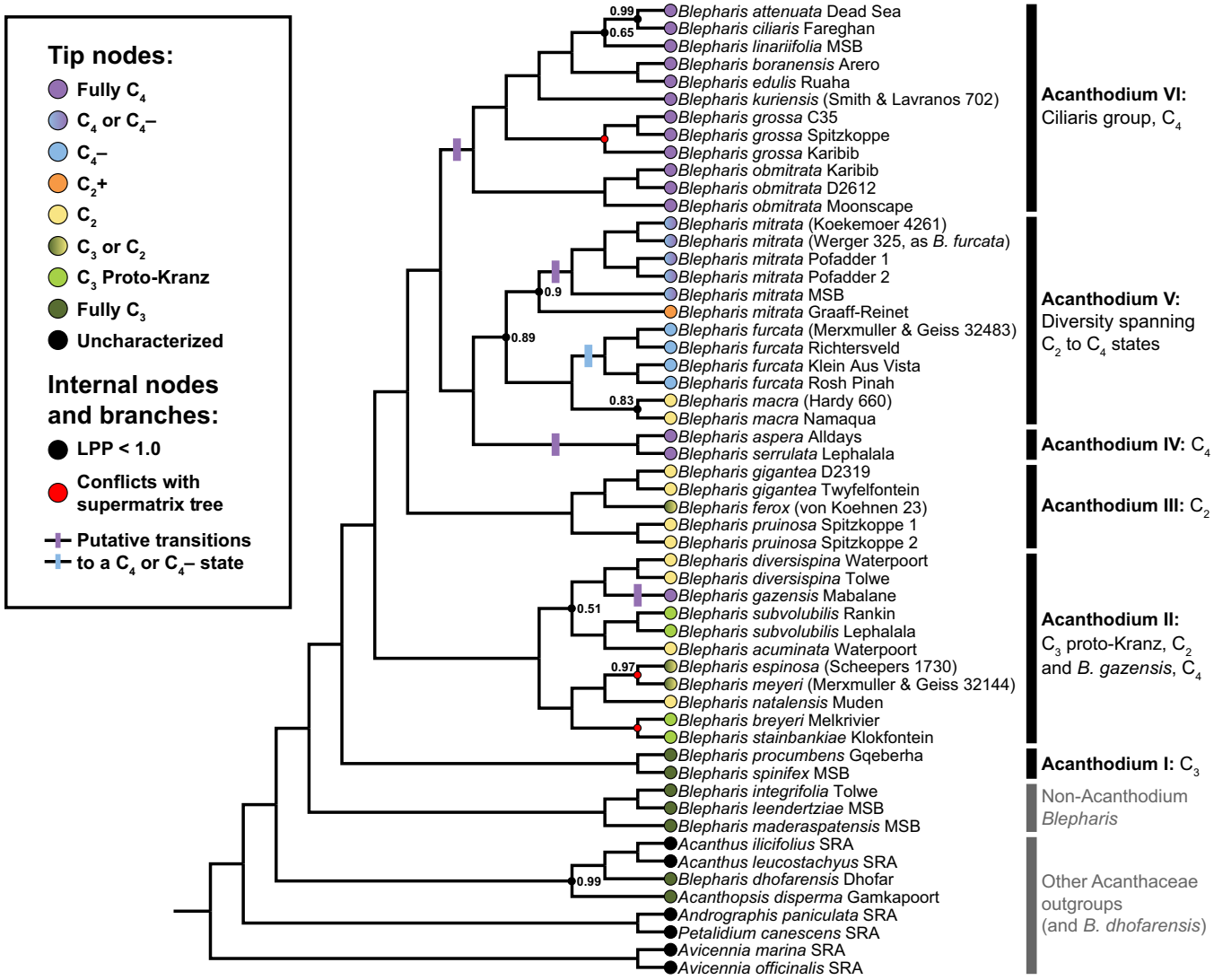

Fig. 10 *Blepharis* species tree summarized from super-matrix and coalescent phylogenetic inference. A summary cladogram for phylogenetic inferences on 2.78 megabases in 2138 loci, using the multispecies coalescent and concatenated super-matrix methods. The node support values shown are local posterior probabilities from the coalescent tree. Nodes without support values indicated have full support from both methods, except for the three nodes marked in red, which represent conflicts between the two trees. The separate coalescent and super-matrix trees are presented in Supporting Information Fig. S6, including quartet support for the coalescent tree. Two populations of *B. capensis* and one population resembling *B. mitrata* were omitted from these analyses due to evidence of hybridization (Notes S1). Several herbarium specimens are included, with the collector's name and number in parentheses. Photosynthetic pathways are inferred for herbarium specimens based on $\delta^{13}C$ values and phylogenetic position.

abundant grana indicate elevated levels of photosystem II and $NADP^+$ reduction (Edwards & Walker, 1983), these results indicate *B. gazensis* utilizes aspartate over malate as the main C_4 transport metabolite, as occurs in NAD-ME C_4 species. Unlike malate, aspartate does not carry reducing power, and C_4 plants that transport aspartate require more photosystem II activity in BS chloroplasts to meet the redox needs of the PCR cycle (Edwards & Walker, 1983; Furbank, 2011). The elevated rates of AST and ALT in *B. gazensis* are consistent with this interpretation (Drincovich *et al.*, 2011). The abundant BS mitochondria are best explained by the use of mitochondrial isoforms of AST and ALT (Stata, 2023). This type of aspartate-dependent NADP-ME C_4 pathway has been hypothesized as feasible but never previously observed and may represent either a transitional stage during the evolution of a more typical NADP-ME C_4 pathway or an uncommon yet stable evolutionary endpoint.

Intraspecific variation spanning from C_2 to C_4 photosynthesis

To investigate intraspecific photosynthetic diversity in the C_4- species identified here and in Fisher *et al.* (2015), we measured $\delta^{13}C$ in herbarium specimens of *B. furcata* and *B. macra* from across their geographical ranges. $\delta^{13}C$ values in *B. furcata* ranged

from −14.6 to −23.0‰ and −16.4 to −27.1‰ in *B. macra*. Together, their values form a gradient from non-C_4 to fully C_4 $\delta^{13}C$ values, with the former likely representing C_2 populations based on phylogenetic distance from C_3 taxa. Most *B. macra* populations have $\delta^{13}C$ values consistent with minimal C_4 cycle activity, but C_4− values occur in three populations.

B. mitrata was classified as C_4 by Fisher *et al.* (2015) based on $\delta^{13}C$ in two specimens; however, we found evidence of variability in this species as well. While two live accessions are C_4, the Graaff-Reinet accession exhibits a C_2+ phenotype. We therefore included 66 *B. mitrata* herbarium specimens in our $\delta^{13}C$ survey. Of these, 28 have non-C_4 $\delta^{13}C$ values (−21 to −30‰), while 35 have C_4 values (−13 to −16‰), with the latter averaging *c.* 1‰ more negative than C_4 values from Fisher *et al.* (2015). Eight specimens had intermediate values (−16 to −22‰), consistent with C_4− physiology. Non-C_4 specimens were predominantly collected below or along South Africa's Great Escarpment, whereas C_4 specimens occurred throughout the range except in the southeastern extreme (Fig. 9). Together, $\delta^{13}C$ data from *B. furcata*, *B. macra*, and *B. mitrata* indicate that C_4 evolution is active and ongoing in these three species, with a gradient of phenotypes spanning the C_2 to C_4 transition.

The phylogenetic context of intermediate phenotypes

The evolutionary significance of the photosynthetic diversity in *Blepharis* is reinforced by our phylogeny, which supports the interpretation of intermediate phenotypes as extant stages of C_4 evolution. The fully C_3 species in sect. *Acanthodium*, *B. procumbens* and *B. spinifex*, form a clade, which we designate Acanthodium I. The basal-branching position of this clade is consistent with the hypothesis of a C_3 ancestral state for sect. *Acanthodium*, extending the range of evolutionary steps present compared with the C_2 ancestral state hypothesized by Fisher *et al.* (2015). A distal clade designated Acanthodium VI comprises most of the fully C_4 taxa in this study. The known C_4 species absent from this study, *B. glinus* and *B. scindica*, likely belong to this clade as well, based on the phylogeny of Fisher *et al.* (2015). Between these clades, the Acanthodium II through V clades comprise groups of intermediates and phylogenetically distinct C_4 and C_4− lineages.

The phylogenetic placement of C_3–C_4 intermediate phenotypes in *Blepharis* highlights their roles as transitional states during C_4 evolution. Apart from *B. gazensis*, the Acanthodium II and III clades reflect the $C_3 \rightarrow$ proto-Kranz $\rightarrow C_2$ transitions. Proto-Kranz *Blepharis* species occupy phylogenetically intermediate positions branching sister to C_3 and C_2 species, a pattern also observed in *Flaveria* (Sage *et al.*, 2013). This supports a model of C_4 evolution in which proto-Kranz anatomy precedes the C_2 phenotype, which then serves as a necessary intermediate to C_4 photosynthesis. Although C_2 photosynthesis is hypothesized to be an essential stage during C_4 evolution, the proto-Kranz and C_2 states may also arise from hybridization between C_3 and C_4 species (Kadereit *et al.*, 2017; Tefarikis *et al.*, 2022; Alvarenga *et al.*, 2025). However, phylogenetic network analysis demonstrates that C_2 physiology in *Blepharis* primarily arose through vertical evolution, supporting the hypothesis that the C_2 state is essential during C_4 evolution (Notes S1). The unusual biochemistry and BS ultrastructure of *B. gazensis* is reflected in its phylogenetic distance from other C_4 *Blepharis* species, nested in the Acanthodium II clade.

Given the lack of evidence for reversion from a C_4 state (Christin *et al.*, 2010; Ingram *et al.*, 2011; Oakley *et al.*, 2014), we identify five putative evolutionary origins of the C_4 cycle in *Blepharis* (Fig. 10). However, given the evidence for a C_4 cycle in at least some populations of all taxa in the Acanthodium IV, V, and VI clades, it is possible that the C_4 cycle emerged in the common ancestor of these clades, with intraspecific variation persisting within *B. furcata*, *B. macra*, and *B. mitrata*. Assuming five C_4 origins, *Blepharis* would be the leading genus for C_4 evolution, exceeding the two to three independent C_4 clades suggested for *Alloteropsis*, *Flaveria*, *Neurachne*, and *Portulaca* (Sage, 2016). *Blepharis* demonstrates that complex trait evolution can be highly dynamic within genera.

C_4 evolution and complex trait assembly

Blepharis supports and extends the stepwise model of C_4 evolution developed in *Flaveria* and other C_3–C_4 transitional lineages (Monson & Rawsthorne, 2000; Sage *et al.*, 2012). C_3 and proto-Kranz species in *Blepharis* sect. *Acanthodium* inhabit hot, dry, and weakly monsoonal climates where photorespiration is high during the growing season (Vollesen, 2000; Fisher *et al.*, 2015; Sage *et al.*, 2018). Photorespiration is widely regarded as a central driver for C_4 evolution, although this hypothesis is not ubiquitously supported (Lundgren & Christin, 2017). High photorespiration creates challenges for C_3 plants beyond restricting photosynthetic efficiency (Ehleringer *et al.*, 1997; Busch *et al.*, 2013). Cleavage of photorespiratory glycine produces ammonia and CO_2, both vulnerable to diffusional loss, with ammonia loss being particularly problematic as it depletes nitrogen, a frequently limiting element. Localizing the release of these molecules to the BS enables plants to more effectively recapture them and thus could enable physiological and structural modifications that lead to C_2 and later C_4 photosynthesis (Mallmann *et al.*, 2014).

C_4 cycle enzymes are proposed to support C_2 photosynthesis by facilitating the refixation and shuttling of photorespiratory nitrogen from BS to M tissues (Mallmann *et al.*, 2014), and their upregulation for these functions may facilitate the assembly of the full C_4 cycle. As the C_4 cycle comes together and begins to supply CO_2 to the PCR cycle in the BS, a positive shift in $\delta^{13}C$ occurs, as has been observed in the C_2+ species *Flaveria ramosissima* and to a lesser degree in *F. floridana* (Monson *et al.*, 1986; Edwards & Ku, 1987; Ku *et al.*, 1991; Alonso-Cantabrana & von Caemmerer, 2016). In contrast, most C_2 species in *Blepharis* do not show significant shifts in $\delta^{13}C$ from typical C_3 values, indicating little if any C_4-PCR cycle integration. This is surprising since in *Flaveria* and *Blepharis* intermediates, the activity of a number of C_4 cycle enzymes increases in concert with increases in PEPC activity, which might indicate gradual upregulation of a C_4 cycle. If upregulation of C_4 cycle enzymes has little effect on net carbon gain or $\delta^{13}C$, then what purpose may it serve? Mallmann *et al.* (2014) and Adachi *et al.* (2023) hypothesize that

the function of the partial upregulation of the C_4 cycle in C_2 species is not to enhance carbon fixation but to promote refixation of photorespired NH_3 in the BS cell and facilitate rapid return of photorespiratory N to M cells. High rates of photorespiration could lead to excessive loss of NH_3 via diffusive efflux unless it is rapidly refixed. The release of photorespiratory NH_3 in the BS helps trap it for reassimilation. However, the product of NH_3 reassimilation is glutamate, and establishing a high concentration in BS cells to support rapid diffusion back to M cells may lead to feedback inhibition of glutamate synthase, slowing N reassimilation and leading to NH_3 loss. This can be avoided by transamination of glutamate to alanine (via ALT) or aspartate (via AST), which diffuse to M cells along their own concentration gradients (Adachi *et al.*, 2023). PEPC could be upregulated to produce carbon skeletons for rapid alanine or aspartate production (Mallmann *et al.*, 2014). Mean ALT and AST activities in *Blepharis* are 40% greater in C_2 than in C_3 species, and linear regressions between PEPC and both ALT and AST activities in the C_3 and C_2 species exhibited steeper positive slopes than those between PEPC and other C_4 cycle enzymes. We interpret this as evidence of coordinated upregulation of ALT, AST, and PEPC, beginning in functionally C_3 species. *Flaveria* exhibits a similar steep rise of ALT and AST activities correlated with PEPC activity in C_3 and C_2 species, leading to greater ALT and AST activities in C_2 than in C_3 species (Adachi *et al.*, 2023). C_2 *Tribulus* species (Zygophyllaceae) also show greater ALT and AST activities than C_3 species (Leung *et al.*, 2024). Together, these findings support the hypothesis that photorespiratory nitrogen scavenging is the primary driver of proto-Kranz and C_2 evolution, and by extension, C_4 evolution, rather than carbon scavenging as hypothesized over a decade ago (Sage *et al.*, 2012).

At the other end of the C_3–C_4 phenotypic spectrum, the Acanthodium V clade comprising *B. furcata*, *B. macra*, and *B. mitrata* exhibits substantial variation spanning C_2 to C_4 phenotypes. This diversity presents an unparalleled opportunity to resolve uncertainty surrounding the later steps in C_4 evolution and their geographic and climatological context. For example, the Great Escarpment of South Africa is a geological feature that extends across southernmost Africa and separates coastal regions from the drier, elevated central plateau in the continental interior (Fig. 7). *B. furcata*, *B. macra*, and *B. mitrata* are distributed across the central plateau, while *B. mitrata* extends further south to below the Great Escarpment (Vollesen, 2000). While C_4 specimens of *B. mitrata* were collected across the species' range, nearly all of the 28 specimens with non-C_4 $\delta^{13}C$ values were collected below or along the Great Escarpment, indicating that C_4 genotypes have expanded geographic and ecological ranges relative to C_2 genotypes, similar to patterns observed in *Alloteropsis* (Lundgren *et al.*, 2015; Sotelo *et al.*, 2024). *B. mitrata* specimens with more C_4-like $\delta^{13}C$ values were also associated with significantly warmer, drier habitats than those with non-C_4 $\delta^{13}C$ values (Fig. S5), indicating ecological niche separation as often described for C_4 vs C_3 species (Ehleringer *et al.*, 1997). The bimodal $\delta^{13}C$ distribution in *B. mitrata* indicates that gene flow between C_4 and non-C_4 populations is reduced, such that C_4 evolution in *B. mitrata* may be linked to partial allopatric speciation; for example, genes with large effects on C_4 physiology could function as barrier loci if interbreeding between C_4 and non-C_4 individuals reduces fitness (Ravinet *et al.*, 2017). In contrast, *B. furcata* and *B. macra* each exhibit continuous $\delta^{13}C$ variation from non-C_4 to fully C_4, with no discernible geographic differences in $\delta^{13}C$ values across their ranges in northwestern South Africa and southwestern Namibia (Vollesen, 2000). Closer examination of the habitat distribution of phenotypes of Acanthodium V species will be needed to determine how climate and geography influence C_4 evolution, a prospect made possible by the diverse character states in this clade. The photosynthetic pathway variation in these three species additionally opens the prospect of within-species genetic crossing and population genomic studies, which up until now have only been possible in *Alloteropsis* (Bianconi *et al.*, 2022; Alenazi *et al.*, 2024).

Conclusion

Blepharis sect. *Acanthodium* includes greater photosynthetic diversity than previously hypothesized, spanning a phenotypic and phylogenetic gradient from C_3 to C_4 photosynthesis. Intermediate character states include proto-Kranz, numerous C_2 species, and a definitive C_4- phenotype previously only reported in *Flaveria*. A novel, predominantly aspartate-shuttling NADP-ME C_4 pathway occurs in *B. gazensis*, a phylogenetically isolated monospecific C_4 lineage.

Intraspecific diversity spanning the gap from C_2 to C_4 photosynthesis is demonstrated in each of *B. furcata*, *B. macra*, and *B. mitrata*, presenting a remarkable opportunity to address major questions of late-stage C_4 evolution. Numerous additional intermediates likely exist, as this study examined only half of all sect. *Acanthodium* species. *Blepharis* thus represents a dynamic system to provide new insights, particularly into how the C_4 pathway has been assembled from an ancestral C_2 state. Parallel study of *Blepharis* and other highly informative C_3-to-C_4 transitional lineages will yield further insight into how a trait as complex as C_4 photosynthesis can evolve with such remarkable frequency.

Acknowledgements

We thank the following individuals for providing germplasm or herbarium materials used in this study: Deb Metsger, Hester Steyn, Iain Darbyshire, Kaj Vollesen, Ton Rulkens, Ina Loots, Roxana Khoshravesh, Spencer Barrett, Gudaina Al-Issai, Brad Ripley, Angela Blane, Janet Terry, Alpheus Mothapo, Nicolien Sol, and Andreas Fleischmann. We also thank Brynmor Crookall, Phaedra Otwey, Ria Patel, Perlina Lim, and Nina Esmail for assistance with microscopy sample preparation, sectioning, and imaging. This research was supported by a CGS-D graduate scholarship from the Natural Sciences and Engineering Research Council of Canada (NSERC), a Queen Elizabeth II Graduate Scholarship in Science and Technology (QEII-GSST), and three Centre for Global Change Science travel awards to MS, plus Natural Sciences and Engineering Research Council of Canada Discovery grants RGPIN-2015-04878 and RGPIN-2020-05925 (consecutively) to TLS and RGPIN-2017-06476 to RFS. All transcriptome sequencing was supported by grants from the Strategic Priority Research Program of the Chinese

Academy of Sciences (XDB0630101 to MJAL and XDB0630301, XGZ), General program of the National Science Foundation of China (31870214 to XGZ), and National Science Foundation grant 31870214 to XGZ. DNA sequencing of herbarium specimens and *B. dhofarensis* was supported by a Guangdong Basic and Applied Basic Research Foundation grant (2022A1515110358) and a National Natural Science Foundation of China grant (32300217) to HL. Computations were performed on the Niagara supercomputer at the SciNet HPC Consortium. SciNet is funded by Innovation, Science and Economic Development Canada; the Digital Research Alliance of Canada; the Ontario Research Fund: Research Excellence; and the University of Toronto. MS is currently supported by the US Department of Energy and US National Science Foundation grants DE-SC0018277 and IOS-2406533 to Seung Yon Rhee at Michigan State University. [Correction added on 27 September 2025, after first online publication: the preceding sentence was added, after previously being omitted in error.]

Competing interests

None declared.

Author contributions

MS, RFS and TLS conceived and designed this study. MS and RFS conducted field collections. MS acquired herbarium samples, performed physiological assessments, sample preparation for microscopy and $\delta^{13}C$ analysis, and transmission electron microscope imaging. TLS conducted light microscopy imaging and created all microscopy figures. MS and M-JAL prepared samples for RNA-seq, and HL prepared samples of herbarium specimens and *B. dhofarensis* for DNA sequencing. MS analyzed the data, generated the figures, and wrote the paper with input from all authors, particularly RFS and TLS. RFS and TLS supervised MS, X-GZ supervised M-JAL and SC supervised HL. MS, RFS, TLS, X-GZ and SC acquired funding for this research.

ORCID

Shifeng Cheng https://orcid.org/0000-0003-1617-1747
Hongbing Liu https://orcid.org/0000-0002-3017-9668
Ming-Ju Amy Lyu https://orcid.org/0000-0003-0845-9767
Rowan F. Sage https://orcid.org/0000-0001-6183-9246
Tammy L. Sage https://orcid.org/0000-0002-7061-832X
Matt Stata https://orcid.org/0000-0002-5744-4898
Xin-Guang Zhu https://orcid.org/0000-0002-4435-130X

Data availability

All datasets, including the supermatrix and all gene trees used for the phylogenetic analyses, are provided in the online Supporting Information (Tables S1–11; Figs S1–S8; Notes S1), Dataset S1 (an Excel file containing all physiological data), and Dataset S2 (a zip archive containing super-matrix sequences, partition information, and gene trees used in all phylogenetic analyses).

References

Adachi S, Stata M, Martin DG, Cheng S, Liu H, Zhu X-G, Sage RF. 2023. The evolution of C_4 photosynthesis in *Flaveria* (Asteraceae): insights from the *Flaveria linearis* complex. *Plant Physiology* **191**: 233–251.

Akhani H, Ghasemkhani M, Chuong SDX, Edwards GE. 2008. Occurrence and forms of Kranz anatomy in photosynthetic organs and characterization of NAD-ME subtype C_4 photosynthesis in *Blepharis ciliaris* (L.) B. L. Burtt (Acanthaceae). *Journal of Experimental Botany* **59**: 1755–1765.

Alenazi AS, Pereira L, Christin P-A, Osborne CP, Dunning LT. 2024. Identifying genomic regions associated with C_4 photosynthetic activity and leaf anatomy in *Alloteropsis semialata*. *New Phytologist* **243**: 1698–1710.

Alonso-Cantabrana H, von Caemmerer S. 2016. Carbon isotope discrimination as a diagnostic tool for C_4 photosynthesis in C_3-C_4 intermediate species. *Journal of Experimental Botany* **67**: 3109–3121.

Alvarenga JP, Stata M, Sage RF, Patel R, das Chagas Mendonca AM, Della Torre F, Liu H, Cheng S, Weake S, Watanabe EJ *et al.* 2025. Evolutionary diversification of C_2 photosynthesis in the grass genus *Homolepis* (Arthropogoninae). *Annals of Botany* **135**: 769–788.

Arnon DI. 1949. Copper enzymes in isolated chloroplasts. Polyphenoloxidase in *Beta vulgaris*. *Plant Physiology* **24**: 1–15.

Ashton AR, Burnell JN, Furbank RT, Jenkins CLD, Hatch MD. 1990. Enzymes of C_4 photosynthesis. In: Lea PJ, ed. *Enzymes of primary metabolism. Methods in plant biochemistry*. Cambridge, MA, USA: Academic Press, 39–72.

Bianconi ME, Sotelo G, Curran EV, Milenkovic V, Samaritani E, Dunning LT, Bertolino LT, Osborne CP, Christin P-A. 2022. Upregulation of C_4 characteristics does not consistently improve photosynthetic performance in intraspecific hybrids of a grass. *Plant, Cell & Environment* **45**: 1398–1411.

Bolger AM, Lohse M, Usadel B. 2014. Trimmomatic: a flexible trimmer for Illumina sequence data. *Bioinformatics* **30**: 2114–2120.

Busch FA, Sage TL, Cousins AB, Sage RF. 2013. C_3 plants enhance rates of photosynthesis by reassimilating photorespired and respired CO_2. *Plant, Cell & Environment* **36**: 200–212.

von Caemmerer S. 1989. A model of photosynthetic CO_2 assimilation and carbon-isotope discrimination in leaves of certain C_3-C_4 intermediates. *Planta* **178**: 463–474.

von Caemmerer S. 1992. Carbon isotope discrimination in C_3-C_4 intermediates. *Plant, Cell & Environment* **15**: 1063–1072.

Capella-Gutiérrez S, Silla-Martínez JM, Gabaldón T. 2009. trimAl: a tool for automated alignment trimming in large-scale phylogenetic analyses. *Bioinformatics* **25**: 1972–1973.

Cheng S-H, Moore BD, Edwards GE, Ku MSB. 1988. Photosynthesis in *Flaveria brownii*, a C_4-like species: leaf anatomy, characteristics of CO_2 exchange, compartmentation of photosynthetic enzymes, and metabolism of $^{14}CO_2$. *Plant Physiology* **87**: 867–873.

Christin P-A, Freckleton RP, Osborne CP. 2010. Can phylogenetics identify C_4 origins and reversals? *Trends in Ecology & Evolution* **25**: 403–409.

Conover WJ, Iman RL. 1979. On multiple comparisons procedures. Technical reports, Los Alamos Scientific Laboratory.

Conway Morris S. 2003. *Life's solution: inevitable humans in a lonely universe*. Cambridge, UK: Cambridge University Press.

Danecek P, Bonfield JK, Liddle J, Marshall J, Ohan V, Pollard MO, Whitwham A, Keane T, McCarthy SA, Davies RM *et al.* 2021. Twelve years of SAMtools and BCFtools. *GigaScience* **10**: giab008.

Darwin C. 1859. *On the origin of species by means of natural selection, or preservation of favoured races in the struggle for life*. London, UK: John Murray.

Dever LV, Boxall SF, Kneřová J, Hartwell J. 2015. Transgenic perturbation of the decarboxylation phase of Crassulacean acid metabolism alters physiology and metabolism but has only a small effect on growth. *Plant Physiology* **167**: 44–59.

Drincovich MF, Lara MV, Andreo CS, Maurino VG. 2011. C_4 decarboxylases: different solutions for the same biochemical problem, the provision of CO_2 to Rubisco in the bundle sheath cells. In: Raghavendra AS, Sage RF, eds. *C_4 photosynthesis and related CO_2 concentrating mechanisms*. Dordrecht, the Netherlands: Springer Netherlands, 277–300.

Dunning LT, Moreno-Villena JJ, Lundgren MR, Dionora J, Salazar P, Adams C, Nyirenda F, Olofsson JK, Mapaura A, Grundy IM *et al.* 2019. Key changes in gene expression identified for different stages of C_4 evolution in *Alloteropsis semialata*. *Journal of Experimental Botany* **70**: 3255–3268.

Edwards G, Walker D. 1983. *C_3, C_4: mechanisms, and cellular and environmental regulation, of photosynthesis*. Berkeley, CA, USA: University of California Press.

Edwards GE, Ku MSB. 1987. Biochemistry of C_3–C_4 intermediates. In: Hatch MD, Boardman NK, eds. *Photosynthesis*. Cambridge, MA, USA: Academic Press, 275–325.

Ehleringer JR, Cerling TE, Helliker BR. 1997. C_4 photosynthesis, atmospheric CO_2, and climate. *Oecologia* **112**: 285–299.

Emms DM, Kelly S. 2019. OrthoFinder: Phylogenetic orthology inference for comparative genomics. *Genome Biology* **20**: 238.

Fisher AE, McDade LA, Kiel CA, Khoshravesh R, Johnson MA, Stata M, Sage TL, Sage RF. 2015. Evolutionary history of *Blepharis* (Acanthaceae) and the origin of C_4 photosynthesis in section *Acanthodium*. *International Journal of Plant Sciences* **176**: 770–790.

Friesen PC, Sage RF. 2016. Photosynthetic responses to chilling in a chilling-tolerant and chillingsensitive *Miscanthus* hybrid. *Plant, Cell & Environment* **39**: 1420–1431.

Furbank RT. 2011. Evolution of the C4 photosynthetic mechanism: are there really three C4 acid decarboxylation types? *Journal of Experimental Botany* **62**: 3103–3108.

Grabherr MG, Haas BJ, Yassour M, Levin JZ, Thompson DA, Amit I, Adiconis X, Fan L, Raychowdhury R, Zeng Q *et al.* 2011. Trinity: reconstructing a full-length transcriptome without a genome from RNA-Seq data. *Nature Biotechnology* **29**: 644–652.

Gutterman Y. 1993. *Seed Germination in Desert Plants*. Berlin, Germany: Springer, 253.

Harmon LJ. 2018. *Phylogenetic comparative methods: learning from trees*. Scotts Valley, CA, USA: CreateSpace Independent Publishing Platform.

Heckmann D, Schulze S, Denton A, Gowik U, Westhoff P, Weber APM, Lercher MJ. 2013. Predicting C_4 photosynthesis evolution: modular, individually adaptive steps on a Mount Fuji fitness landscape. *Cell* **153**: 1579–1588.

Ingram AL, Christin P-A, Osborne CP. 2011. Molecular phylogenies disprove a hypothesized C_4 reversion in *Eragrostis walteri* (Poaceae). *Annals of Botany* **107**: 321–325.

Kadereit G, Bohley K, Lauterbach M, Tefarikis DT, Kadereit JW. 2017. C_3-C_4 intermediates may be of hybrid origin - a reminder. *New Phytologist* **215**: 70–76.

Katoh K, Standley DM. 2013. MAFFT multiple sequence alignment software version 7: improvements in performance and usability. *Molecular Biology and Evolution* **30**: 772–780.

Keys AJ, Parry MAJ. 1990. Ribulose bisphosphate carboxylase/oxygenase and carbonic anhydrase. In: Lea PJ, ed. *Enzymes of primary metabolism. Methods in plant biochemistry*. Cambridge, MA, USA: Academic Press, 1–14.

Khoshravesh R, Lundsgaard-Nielsen V, Sultmanis S, Sage TL. 2017. Light microscopy, transmission electron microscopy, and immunohistochemistry protocols for studying photorespiration. *Methods in Molecular Biology* **1653**: 243–270.

Khoshravesh R, Stata M, Adachi S, Sage TL, Sage RF. 2020a. Evolutionary convergence of C_4 photosynthesis: a case study in the Nyctaginaceae. *Frontiers in Plant Science* **11**: 578739.

Khoshravesh R, Stata M, Busch FA, Saladié M, Castelli JM, Dakin N, Hattersley PW, Macfarlane TD, Sage RF, Ludwig M *et al.* 2020b. The evolutionary origin of C_4 photosynthesis in the grass subtribe Neurachninae. *Plant Physiology* **182**: 566–583.

Khoshravesh R, Stinson CR, Stata M, Busch FA, Sage RF, Ludwig M, Sage TL. 2016. C_3-C_4 intermediacy in grasses: organelle enrichment and distribution, glycine decarboxylase expression, and the rise of C_2 photosynthesis. *Journal of Experimental Botany* **67**: 3065–3078.

Kim D, Paggi JM, Park C, Bennett C, Salzberg SL. 2019. Graph-based genome alignment and genotyping with HISAT2 and HISAT-genotype. *Nature Biotechnology* **37**: 907–915.

Kozlov AM, Darriba D, Flouri T, Morel B, Stamatakis A. 2019. RAxML-NG: a fast, scalable and user-friendly tool for maximum likelihood phylogenetic inference. *Bioinformatics* **35**: 4453–4455.

Kruskal WH, Wallis WA. 1952. Use of ranks in one-criterion variance analysis. *Journal of the American Statistical Association* **47**: 583–621.

Ku M, Monson R, Littlejohn R, Nakamoto H, Fisher D, Edwards G. 1983. Photosynthetic characteristics of C_3-C_4 intermediate *Flaveria* species 1: leaf anatomy, photosynthetic responses to O_2 and CO_2, and activities of key enzymes in the C_3 and C_4 pathways. *Plant Physiology* **71**: 944–948.

Ku MS, Wu J, Dai Z, Scott RA, Chu C, Edwards GE. 1991. Photosynthetic and photorespiratory characteristics of *Flaveria* species. *Plant Physiology* **96**: 518–528.

Leung A, Patel R, Chirachon V, Stata M, Macfarlane TD, Ludwig M, Busch FA, Sage TL, Sage RF. 2024. *Tribulus* (Zygophyllaceae) as a case study for the evolution of C_2 and C_4 photosynthesis. *Plant, Cell & Environment* **47**: 3541–3560.

Liu H, Zhao H, Zhang Y, Li X, Zuo Y, Wu Z, Jin K, Xian W, Wang W, Ning W *et al.* 2024. The genome of *Eleocharis vivipara* elucidates the genetics of C_3-C_4 photosynthetic plasticity and karyotype evolution in the Cyperaceae. *Journal of Integrative Plant Biology* **66**: 2505–2527.

Losos JB. 2011. Convergence, adaptation, and constraint. *Evolution; International Journal of Organic Evolution* **65**: 1827–1840.

Losos JB. 2018. *Improbable destinies: fate, chance, and the future of evolution*. New York, NY, USA: Riverhead Books.

Lundgren MR, Besnard G, Ripley BS, Lehmann CER, Chatelet DS, Kynast RG, Namaganda M, Vorontsova MS, Hall RC, Elia J *et al.* 2015. Photosynthetic innovation broadens the niche within a single species. *Ecology Letters* **18**: 1021–1029.

Lundgren MR, Christin P-A. 2017. Despite phylogenetic effects, C_3-C_4 lineages bridge the ecological gap to C_4 photosynthesis. *Journal of Experimental Botany* **68**: 241–254.

Lundgren MR, Christin P-A, Escobar EG, Ripley BS, Besnard G, Long CM, Hattersley PW, Ellis RP, Leegood RC, Osborne CP. 2016. Evolutionary implications of C_3-C_4 intermediates in the grass *Alloteropsis semialata*. *Plant, Cell & Environment* **39**: 1874–1885.

Lundgren MR, Dunning LT, Olofsson JK, Moreno-Villena JJ, Bouvier JW, Sage TL, Khoshravesh R, Sultmanis S, Stata M, Ripley BS *et al.* 2019. C_4 anatomy can evolve via a single developmental change. *Ecology Letters* **22**: 302–312.

MacQueen J. 1967. Some methods for classification and analysis of multivariate observations. *Proceedings of the Fifth Berkeley Symposium on Mathematical Statistics and Probability, Volume 1: Statistics* **5.1**: 281–298.

Mallmann J, Heckmann D, Bräutigam A, Lercher MJ, Weber APM, Westhoff P, Gowik U. 2014. The role of photorespiration during the evolution of C_4 photosynthesis in the genus *Flaveria*. *eLife* **3**: e02478.

Matsuba K, Imaizumi N, Kaneko S, Samejima M, Ohsugi R. 1997. Photosynthetic responses to temperature of phosphoenolpyruvate carboxykinase type C_4 species differing in cold sensitivity. *Plant, Cell & Environment* **20**: 268–274.

McDade LA, Daniel TF, Kiel CA, Vollesen K. 2005. Phylogenetic relationships among Acantheae (Acanthaceae): major lineages present contrasting patterns of molecular evolution and morphological differentiation. *Systematic Botany* **30**: 834–862.

McKown AD, Moncalvo J-M, Dengler NG. 2005. Phylogeny of *Flaveria* (Asteraceae) and inference of C_4 photosynthesis evolution. *American Journal of Botany* **92**: 1911–1928.

McKown AD, Dengler NG. 2007. Key innovations in the evolution of Kranz anatomy and C_4 vein pattern in *Flaveria* (Asteraceae). *American Journal of Botany* **94**: 382–399.

Monson RK, Edwards GE, Ku MSB. 1984. C_3-C_4 intermediate photosynthesis in plants. *Bioscience* **34**: 563–574.

Monson RK, Moore BD, Ku MS, Edwards GE. 1986. Co-function of C_3-and C_4-photosynthetic pathways in C_3, C_4 and C_3-C_4 intermediate *Flaveria* species. *Planta* **168**: 493–502.

Monson RK, Rawsthorne S. 2000. CO_2 assimilation in C_3-C_4 intermediate plants. In: Leegood RC, Sharkey TD, von Caemmerer S, eds. *Advances in Photosynthesis and Respiration: Photosynthesis: Physiology and Metabolism*. Dordrecht, the Netherlands: Springer Netherlands, 533–550.

Monson RK, Schuster WS, Ku MS. 1987. Photosynthesis in *Flaveria brownii* A.M. Powell: a C_4like C_3-C_4 intermediate. *Plant Physiology* **85**: 1063–1067.

Monson RK, Teeri JA, Ku MS, Gurevitch J, Mets LJ, Dudley S. 1988. Carbon-isotope discrimination by leaves of *Flaveria* species exhibiting different amounts of C_3-and C_4-cycle cofunction. *Planta* **174**: 145–151.

Moore BD, Ku MSB, Edwards GE. 1989. Expression of C_4-like photosynthesis in several species of *Flaveria*. *Plant, Cell & Environment* **12**: 541–549.

Moore BD, Monson RK, Ku MSB, Edwards GE. 1988. Activities of principal photosynthetic and photorespiratory enzymes in leaf mesophyll and bundle sheath protoplasts from the C_3-C_4 intermediate *Flaveria ramosissima*. *Plant and Cell Physiology* **29**: 999–1006.

Muhaidat R, Sage RF, Dengler NG. 2007. Diversity of kranz anatomy and biochemistry in C_4 eudicots. *American Journal of Botany* **94**: 362–381.

Muhaidat R, Sage TL, Frohlich MW, Dengler NG, Sage RF. 2011. Characterization of C_3–C_4 intermediate species in the genus *Heliotropium* L. (Boraginaceae): anatomy, ultrastructure and enzyme activity. *Plant, Cell & Environment* **34**: 1723–1736.

Niklaus M, Kelly S. 2019. The molecular evolution of C_4 photosynthesis: opportunities for understanding and improving the world's most productive plants. *Journal of Experimental Botany* **70**: 795–804.

Oakley JC, Sultmanis S, Stinson CR, Sage TL, Sage RF. 2014. Comparative studies of C_3 and C_4 *Atriplex* hybrids in the genomics era: physiological assessments. *Journal of Experimental Botany* **65**: 3637–3647.

Pedregosa F, Varoquaux G, Gramfort A, Michel V, Thirion B, Grisel O, Blondel M, Prettenhofer P, Weiss R, Dubourg V *et al.* 2011. Scikit-learn: machine learning in Python. *The Journal of Machine Learning Research* **12**: 2825–2830.

Pereira L, Bianconi ME, Osborne CP, Christin P-A, Dunning LT. 2023. *Alloteropsis semialata* as a study system for C_4 evolution in grasses. *Annals of Botany* **132**: 365–381.

Ravinet M, Faria R, Butlin RK, Galindo J, Bierne N, Rafajlović M, Noor MAF, Mehlig B, Westram AM. 2017. Interpreting the genomic landscape of speciation: a road map for finding barriers to gene flow. *Journal of Evolutionary Biology* **30**: 1450–1477.

Rawsthorne S. 1992. C_3–C_4 intermediate photosynthesis: linking physiology to gene expression. *The Plant Journal* **2**: 267–274.

Rice P, Longden I, Bleasby A. 2000. EMBOSS: the European molecular biology open software suite. *Trends in Genetics* **16**: 276–277.

Richter A, Wanek W, Werner RA, Ghashghaie J, Jäggi M, Gessler A, Brugnoli E, Hettmann E, Göttlicher SG, Salmon Y. 2009. Preparation of starch and soluble sugars of plant material for the analysis of carbon isotope composition: a comparison of methods. *Rapid Communications in Mass Spectrometry* **23**: 2476–2488.

Sage TL, Sage RF, Vogan PJ, Rahman B, Johnson DC, Oakley JC, Heckel MA. 2011. The occurrence of C_2 photosynthesis in *Euphorbia* subgenus *Chamaesyce* (Euphorbiaceae). *Journal of Experimental Botany* **62**: 3183–3195.

Sage RF. 2016. A portrait of the C_4 photosynthetic family on the 50th anniversary of its discovery: species number, evolutionary lineages, and Hall of Fame. *Journal of Experimental Botany* **67**: 4039–4056.

Sage RF, Khoshravesh R, Sage TL. 2014. From proto-kranz to C_4 kranz: building the bridge to C_4 photosynthesis. *Journal of Experimental Botany* **65**: 3341–3356.

Sage RF, Sage TL, Kocacinar F. 2012. Photorespiration and the evolution of C_4 photosynthesis. *Annual Review of Plant Biology* **63**: 19–47.

Sage TL, Busch FA, Johnson DC, Friesen PC, Stinson CR, Stata M, Sultmanis S, Rahman BA, Rawsthorne S, Sage RF. 2013. Initial events during the evolution of C_4 photosynthesis in C_3 species of *Flaveria*. *Plant Physiology* **163**: 1266–1276.

Sage RF, Monson RK, Ehleringer JR, Adachi S, Pearcy RW. 2018. Some like it hot: the physiological ecology of C_4 plant evolution. *Oecologia* **187**: 941–966.

Sankhla N, Ziegler H, Vyas OP, Stichler W, Trimborn P. 1975. Eco-physiological studies on Indian arid zone plants: V. a screening of some species for the C_4-pathway of photosynthetic CO_2fixation. *Oecologia* **21**: 123–129.

Schindelin J, Rueden CT, Hiner MC, Eliceiri KW. 2015. The ImageJ ecosystem: an open platform for biomedical image analysis. *Molecular Reproduction and Development* **82**: 518–529.

Schulze S, Mallmann J, Burscheidt J, Koczor M, Streubel M, Bauwe H, Gowik U, Westhoff P. 2013. Evolution of C_4 photosynthesis in the genus *Flaveria*: establishment of a photorespiratory CO_2 pump. *Plant Cell* **25**: 2522–2535.

Sotelo G, Gamboa S, Dunning LT, Christin P-A, Varela S. 2024. C_4 photosynthesis provided an immediate demographic advantage to populations of the grass *Alloteropsis semialata*. *New Phytologist* **242**: 774–785.

Stata M, Sage TL, Sage RF. 2019. Mind the gap: the evolutionary engagement of the C_4 metabolic cycle in support of net carbon assimilation. *Current Opinion in Plant Biology* **49**: 27–34.

Stata M. 2023. *The evolution of C4 photosynthesis in Blepharis (Acanthaceae): multiple C4 origins, diverse intermediate states, and divergent routes to a convergent phenotype*. Degree of Doctor of Philosophy, Department of Ecology and Evolutionary Biology, University of Toronto, Toronto, ON, Canada.

Stroud JT, Losos JB. 2016. Ecological opportunity and adaptive radiation. *Annual Review of Ecology, Evolution, and Systematics* **47**: 507–532.

Suyama M, Torrents D, Bork P. 2006. PAL2NAL: robust conversion of protein sequence alignments into the corresponding codon alignments. *Nucleic Acids Research* **34**: W609–W612.

Tefarikis DT, Morales-Briones DF, Yang Y, Edwards G, Kadereit G. 2022. On the hybrid origin of the C_2 *Salsola divaricata* Agg. (Amaranthaceae) from C_3 and C_4 parental lineages. *New Phytologist* **234**: 1876–1890.

Ueno O, Sentoku N. 2006. Comparison of leaf structure and photosynthetic characteristics of C_3 and C_4 *Alloteropsis semialata* subspecies. *Plant, Cell & Environment* **29**: 257–268.

Virtanen P, Gommers R, Oliphant TE, Haberland M, Reddy T, Cournapeau D, Burovski E, Peterson P, Weckesser W, Bright J *et al.* 2020. SciPy 1.0: fundamental algorithms for scientific computing in Python. *Nature Methods* **17**: 261–272.

Vollesen K. 2000. *Blepharis: a taxonomic revision*. London, UK: Kew Royal Botanic Gardens.

Voznesenskaya EV, Artyusheva EG, Franceschi VR, Pyankov VI, Kiirats O, Ku MSB, Edwards GE. 2001. *Salsola arbusculiformis*, a C3−C4 intermediate in Salsoleae (Chenopodiaceae). *Annals of Botany* **88**: 337–348.

Voznesenskaya EV, Koteyeva NK, Akhani H, Roalson EH, Edwards GE. 2013. Structural and physiological analyses in Salsoleae (Chenopodiaceae) indicate multiple transitions among C_3, intermediate, and C_4 photosynthesis. *Journal of Experimental Botany* **64**: 3583–3604.

Yoder JB, Clancey E, Roches SD, Eastman JM, Gentry L, Godsoe W, Hagey TJ, Jochimsen D, Oswald BP, Robertson J *et al.* 2010. Ecological opportunity and the origin of adaptive radiations. *Journal of Evolutionary Biology* **23**: 1581–1596.

Zhang C, Rabiee M, Sayyari E, Mirarab S. 2018. ASTRAL-III: polynomial time species tree reconstruction from partially resolved gene trees. *BMC Bioinformatics* **19**: 153.

Supporting Information

Additional Supporting Information may be found online in the Supporting Information section at the end of the article.

Dataset S1 An Excel file of all physiological data.

Dataset S2 A Zip file archive containing the supermatrix and gene tree files used for all phylogenetic analyses.

Fig. S1 Photographs of *Blepharis* plants and habitats.

Fig. S2 Bar plots of biochemical and physiological parameters in Tables S7–S8.

Fig. S3 Relationship between the activity of PEP carboxylase and other enzymes (C_3 and C_2 species).

Fig. S4 Light micrographs illustrating leaf cross sections across photosynthetic phenotypes.

Fig. S5 Comparison of *Blepharis mitrata* herbarium $\delta^{13}C$ values against climate variables.

Fig. S6 Comparison between coalescent and supermatrix phylogenies.

Fig. S7 *Blepharis* phylogenetic network analyses.

Fig. S8 Pseudo-log-likelihood slope heuristic used in phylogenetic network inference.

Notes S1 Analysis of hybridization in *Blepharis* section *Acanthodium*.

Table S1 Collection information for all species/populations studied.

Table S2 Photosynthetic gas exchange auto-programs used for A/C_i analyses.

Table S3 $\delta^{13}C$ values for herbarium specimens of *Blepharis furcata*, *B. macra*, and *B. mitrata*.

Table S4 Buffers used for extraction of leaves and enzyme assays.

Table S5 All samples used in phylogenetic analyses.

Table S6 Summary of software tools used.

Table S7 Carbon isotope ratio and gas exchange values by species/population.

Table S8 Activity of Rubisco and C_4 cycle enzymes on a Chl basis by species/populations.

Table S9 Activity of Rubisco and C_4 cycle enzymes on a leaf area basis by species/populations.

Table S10 Genome sizes estimated by flow cytometry.

Table S11 Sample inclusion and grouping for phylogenetic network analysis.

Please note: Wiley is not responsible for the content or functionality of any Supporting Information supplied by the authors. Any queries (other than missing material) should be directed to the *New Phytologist* Central Office.

See also the Commentary on this article by Bianconi *et al.*, **248**: 1609–1611.